Project**: SEAWave**

Generic model for estimating occupational exposure

Work Package: WP2

Deliverable: D2.2

Deliverable No.: D6

Abstract

This deliverable discusses the results obtained in the SEAWAVE Tasks 2.2 and 2.3. After confirming the validity of the different simulation tools used by the different partners, a large set of exposure simulation tools in industrial environments was conducted. We provided an extensive discussion of the different scenarios: electric-field or incident power density levels are determined, analyzed, and compared among the different environments and deployments, for the FR1 and FR2 frequency bands. Next, we took the first steps towards a generic model that allows estimating the exposure in industrial environments, only based on inputs that are available to -and understandable for- laymen users. After conducting a correlation analysis between various relevant input and output parameters, a machine-learning based model was constructed building on a large number of simulated scenarios. Promising results were obtained, showing that with a limited amount of high-level information, it is possible to obtain a good indication of exposure levels in the industrial environment.

Project Details

Project name	SEAWave
Grant number	101057622
Start Date	01 Jun 2022
Duration	36 months (extended to 42 months)
Scientific coordinator	Prof. Samaras T, Aristotle University of Thessaloniki (AUTH)

Deliverable Details

Deliverable related number	D2.2
Deliverable No.	D6
Deliverable name	Generic model for estimating occupational exposure
Work Package number	WP2
Work Package name	Occupational Exposures from New 5G Local Networks in Workplaces
Authors	Plets D, Valič B, Apostolidis C, Wang S, Gajšek P
Distribution	Public
Version	Ver 1.0
Draft/final	Final
Keywords	Industry 4.0, Occupational EMF exposure, machine learning

Contents

1 Introduction

This deliverable discusses the results obtained in the SEAWAVE Tasks 2.2 and 2.3. Before delving into the simulation of different environments and the creation of a generic model, Section 2 first describes the exposure simulation tools used in this task, along with an assessment of the similarity of their outputs. This gives us a solid scientific confirmation of the validity of the different tools used. Next, Section 3 treats in detail the industrial simulation scenarios that were investigated by the different WP2 partners. Electric-field or incident power density levels are determined, analyzed, and compared among the different environments and deployments. Section 4 then describes the construction of a generic model that allows estimating the exposure in industrial environments, only based on inputs that are available to -and understandable for- laymen users. The section discusses its performance and its limitations.

2 Exposure simulation tools

Before describing the different simulation scenarios, we present an overview of the simulation tools that were used.

A first tool is the **NARDA simulation tool**. The program package Narda EFC 400 is based on a ray tracing algorithm, and it uses a synthetic model for improved accuracy of near-field calculations according to the IEC 62232:2022 standard, see chapter 6.1.5.7 and B.7.2. The program package incorporates the multiple rays method and considers multiple reflections from object surfaces as well as attenuation and diffuse reflection by objects. The model includes all of the necessary technical data of the pico Remote Radio Heads (pRRHs) as well as the geometry of the surrounding. The attenuation loss is defined individually for each object, but the Narda EFC 400 program package applies a single reflectance value to all objects except for the ground. The calculations include 5 reflections. Material properties for the model are taken from the database within the Narda EFC 400 program package. For example, for solid concrete floor, a reflection coefficient of 0.35 is used, while for concrete walls the reflection coefficient is 0.20. For complex geometries it is necessary to use simplified objects, for example, pallet racks have to be modelled as a solid block with one attenuation loss.

The numerical tool developed in **MATLAB** utilizes MATLAB's built-in ray tracing propagation model to identify the line-of-sight (LOS) and non-line-of-sight (NLOS) propagation paths between the transmitters and the receivers within a 3D model of the environment, which -in this work- is created using Blender software Ver 4.4. For NLOS paths, the model implements the Shooting and Bouncing Rays (SBR) method, where a number of uniformly spaced rays are launched from the transmitter and reflected by surrounding objects. If a ray strikes a flat surface, it reflects and if it strikes an edge, it generates several diffracted rays in accordance with the law of diffraction. For

each ray that reaches a receiver, the total path loss PL is then calculated, which includes the free space, the reflection loss and the diffraction loss.

Reflection and diffraction losses are calculated using the Fresnel equations and the Uniform Theory of Diffraction (UTD), respectively, and depend on the geometry and the electromagnetic properties of the materials defined in the environment's 3D model.

Considering the transmitter output power and its gain in the direction of the receiver, the received power of each ray, P_{ray}, is calculated as:

$$P_{ray}[dBm] = P_{tx}[dBm] + G_{tx,ray}[dB] - PL_{ray}[dB]$$

where P_{tx} is the transmitter input power and $G_{tx,ray}$ is the antenna gain in the direction of the ray. The received power of each ray is then converted to Watts ($P_{ray}[W] = 10^{(P_{ray,dBm}-30)/10}$). Note that as we calculate the total electric field from these received power values, we assumed an isotropic receiver antenna in the equations above. Two subcases of the Matlab RT tool were implemented, depending on whether the rays' phase shift was were taken into account:

A. Power sum

The total received power is obtained by summing the power of all *N* rays:

$$P_{tot}[W] = \sum_{ray=1}^{N} P_{ray}$$

The corresponding total electric field is then:

$$E_{tot}[V/m] = \sqrt{\frac{4\pi Z_0 P_{tot}}{\lambda^2}}$$

where λ is the wavelength (in meters), and Z_0 is the impedance of free space (in ohms).

B. Phasor sum

In the second implementation of the Matlab RT tool, the phase shift of each ray is considered, and the total electric field is obtained as:

$$E_{tot} = \sqrt{\frac{4\pi Z_0}{\lambda^2}} \cdot \left| \sum_{ray=1}^{N} \sqrt{P_{ray}} \cdot e^{i\theta_{ray}} \right|$$

where ϑ_{ray} (=2πd/λ, d being the ray's propagation distance) is the phase shift of the *ray* and *i* is the imaginary unit.

WAVES's Heuristic Indoor Propagation Prediction (**WHIPP**) tool is imec's in-house developed software [Plets], a wireless coverage estimation and network planning suite, allowing the definition and evaluation of different path loss models in tailor-made environments. The coverage calculation is based on a floor plan of the building, which can be obtained by (a) drawing a floor plan of the environment via the user interface, selecting from different building materials, (b) importing existing ground plans, or (c) tracing image scans, whereby an image scan of the floor plan is displayed in the background, allowing the user to easily trace the walls, using the appropriate length scale.

2.1 FR1: 3.5 GHz – common scenario description (INIS-IMEC-AUTH)

The main purpose of the common scenario is to validate all numerical tools used for numerical modelling by all partners. The common scenario is based on the private 5G FR1 base station located in Port of Koper, Slovenia. The real setup was used as a test network for the 5G-LOGINNOV project [5G-LOGINNOV]. The test setup uses an Alpha Wireless AW 3232 directional antenna. The base station configuration is 2×2 with the maximum power of 2×20 W. However, it normally operates at 2×2 W, which is more appropriate for an indoor installation.

The main purpose of the common scenario is to have a simple but precise geometry that is modeled by different collaborators for model validation. Therefore, two common scenarios were defined, with the same base station parameters but with slightly different geometry. One geometry is simple free space situation, whereas the second geometry is a case of indoor installation with two metallic objects inside the building. This geometry is shown in Figure 1. The figure on the left represents an open space without any clutter; the figure on the right contains two metallic objects inside the building.

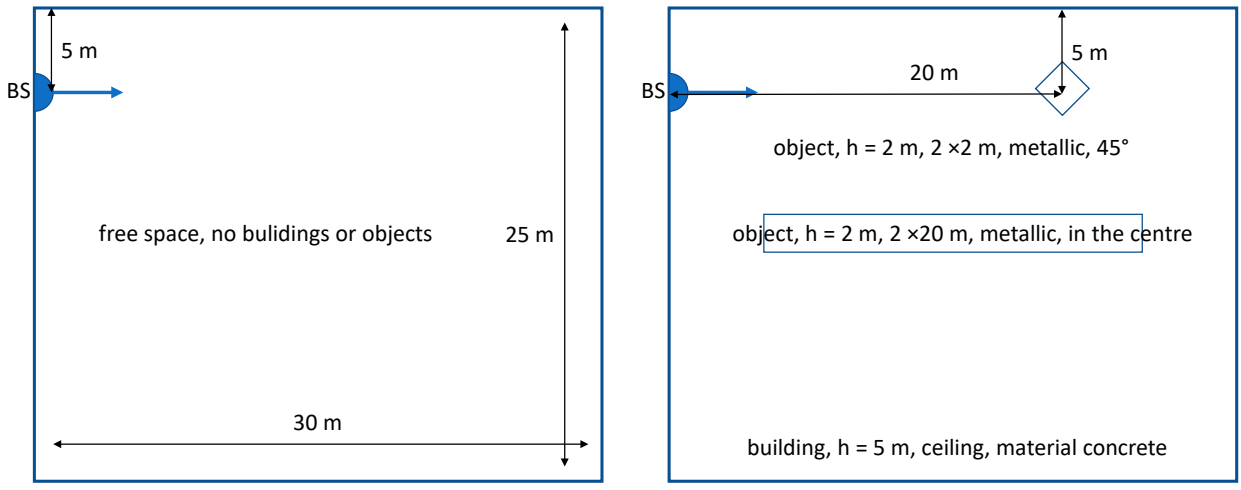

Figure 1. Geometry for the common scenario: open space (left), with two metallic objects (right).

Both common scenarios were calculated by INIS, AUTH and IMEC. Different partners used different tools for numerical calculations. INIS used commercial program package Narda EFC 400, whereas IMEC and AUTH used the MATLAB ray tracing tool (using power sum and phasor sum respectively). In MATLAB, the number of diffractions was set to zero.

The above description of modelling techniques is valid also for other scenarios, if not stated differently.

2.2 FR1: 3.5 GHz – common scenario results (INIS-IMEC-AUTH)

Both common scenarios were calculated by one partner with Narda EFC 400 program package and by two partners with Matlab ray tracing tool and the results were compared. Note that measurement data are provided in D2.3, and comparison between measurements and calculations in D2.4.

2.2.1 NARDA EFC 400 simulation

Both common scenarios were calculated by the resolution of 0.1 m, meaning that the results consist of 75 551 calculation points for open space common scenario (Figure 2, left) and 69 809 points for the cluttered indoor scenario (Figure 2, right). The reason for slightly lower number of calculation points in indoor common scenario is the fact that inside the walls and objects, the field values were not calculated.

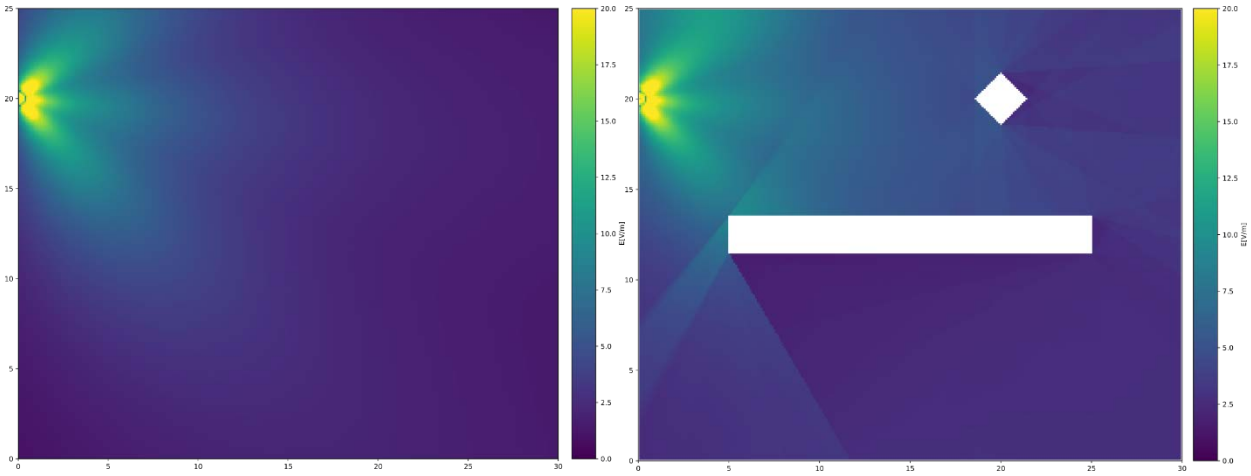

Figure 2. Electric field for common scenario: open space (left), cluttered scenario (right).

For the open space scenario, over all calculated 75 551 points, the maximum value is 46.25 V/m, the 95th percentile is 8.43 V/m, mean value 4.11 V/m, median value 2.31 V/m and standard deviation 6.30 V/m.

For the cluttered indoor scenario, over all calculated 69 809 points, the maximum value is 50.48 V/m, the 95th percentile is 9.81 V/m, mean value 5.15 V/m, median value 3.30 V/m and standard deviation 6.71 V/m.

2.2.2 MATLAB ray-tracing simulation (phasor sum)

Both common scenarios were calculated by the resolution of 0.1 m, meaning that the results consist of 75 000 calculation points for open space common scenario (Figure 3, left) and 70 798 points for the cluttered indoor scenario (Figure 3, right). The reason for slightly lower number of calculation points in indoor common scenario is the fact that inside the walls and objects, the field values are not calculated.

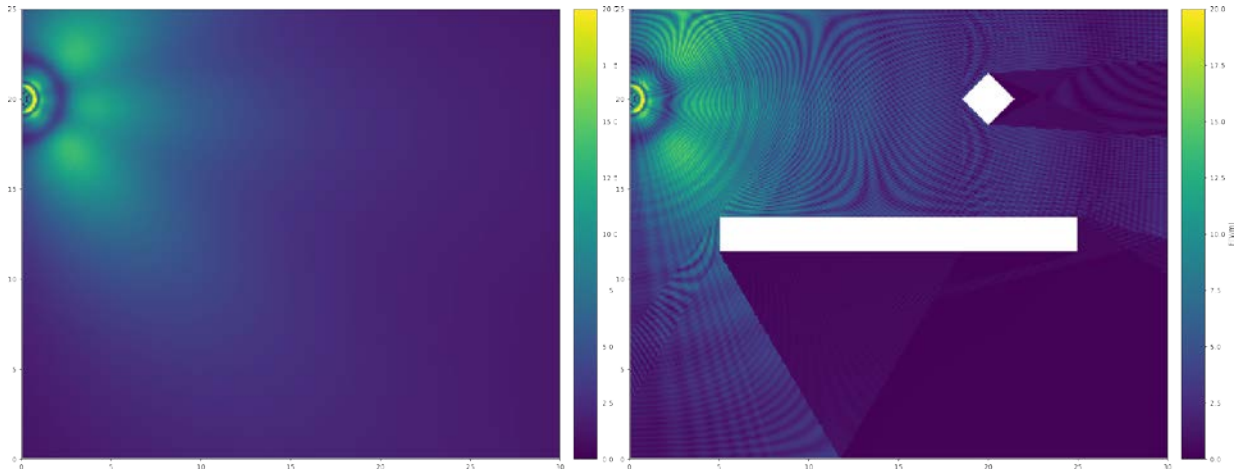

Figure 3. Electric field for common scenario: open space (left), cluttered scenario (right).

Cluttered scenario on the right of Figure 3 was deliberately calculated taking into account phases to analyze the influence of interferences. For the open space scenario, over all calculated 75 000 points, the maximum value is 26.00 V/m, the 95th percentile is 9.43 V/m, mean value 4.27 V/m, median value 2.52 V/m and standard deviation 5.59 V/m. For the cluttered indoor scenario, over all calculated 70 798 points, the maximum value is 26.55 V/m, the 95th percentile is 9.74 V/m, mean value 4.18 V/m, median value 1.72 V/m and standard deviation 5.99 V/m.

2.2.3 MATLAB ray-tracing simulation (power sum)

Both common scenarios were calculated by the resolution of 0.3 m for open space common scenario, which consist of 18 476 calculation points (Figure 4, left) and by the resolution of 0.1 m for the cluttered indoor scenario, which consist of 69 202 calculation points (Figure 4, right).

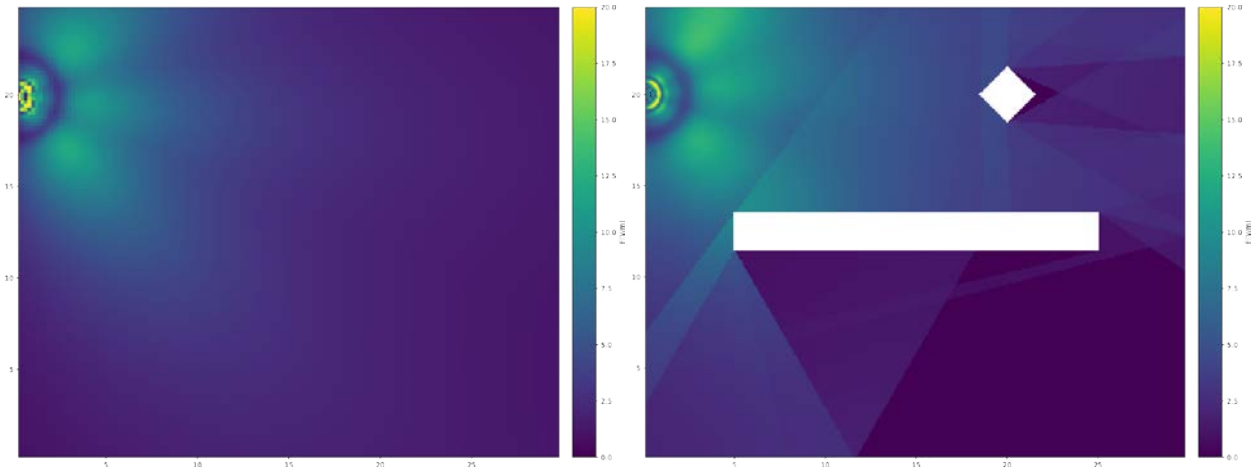

Figure 4: Electric field for common scenario: open space (left), cluttered scenario (right).

For the open space scenario, over all calculated 18 476 points, the maximum value is 26.78 V/m, the 95th percentile is 8.36 V/m, mean value 3.80 V/m, median value 2.23 V/m and standard deviation 5.14 V/m. For the cluttered indoor scenario, over all calculated 69 202 points, the maximum value is 23.82 V/m, the 95th percentile is 9.96 V/m, mean value 4.66 V/m, median value 2.69 V/m and standard deviation 5.90 V/m.

2.2.4 Comparison and discussion

Results of all numerical tools are compared in Figures 5 and 6. Matlab ray tracing simulations did not use segmentation to improve near field calculation accuracy, therefore Narda EFC 400 calculation was performed two times, once without segmentation and once using 8 segments for the antenna. From the Figure 5 and Table 1 for the open space common scenario we can see that all non-segmented results match very well, the segmented result differ significantly up to the distance of 5 m, but for distances greater than 10 m there is no difference between segmented and non-segmented results. From the results in Table 1 we can see that segmented results differ significantly for the maximum value, which can be expected, but for all other statistical values the differences between the models are low. Differences in calculation resolution (Matlab 1 was calculated by the resolution of 0.1 m and Matlab 2 was calculated by the resolution of 0.3 m) didn't have significant influence on the results.

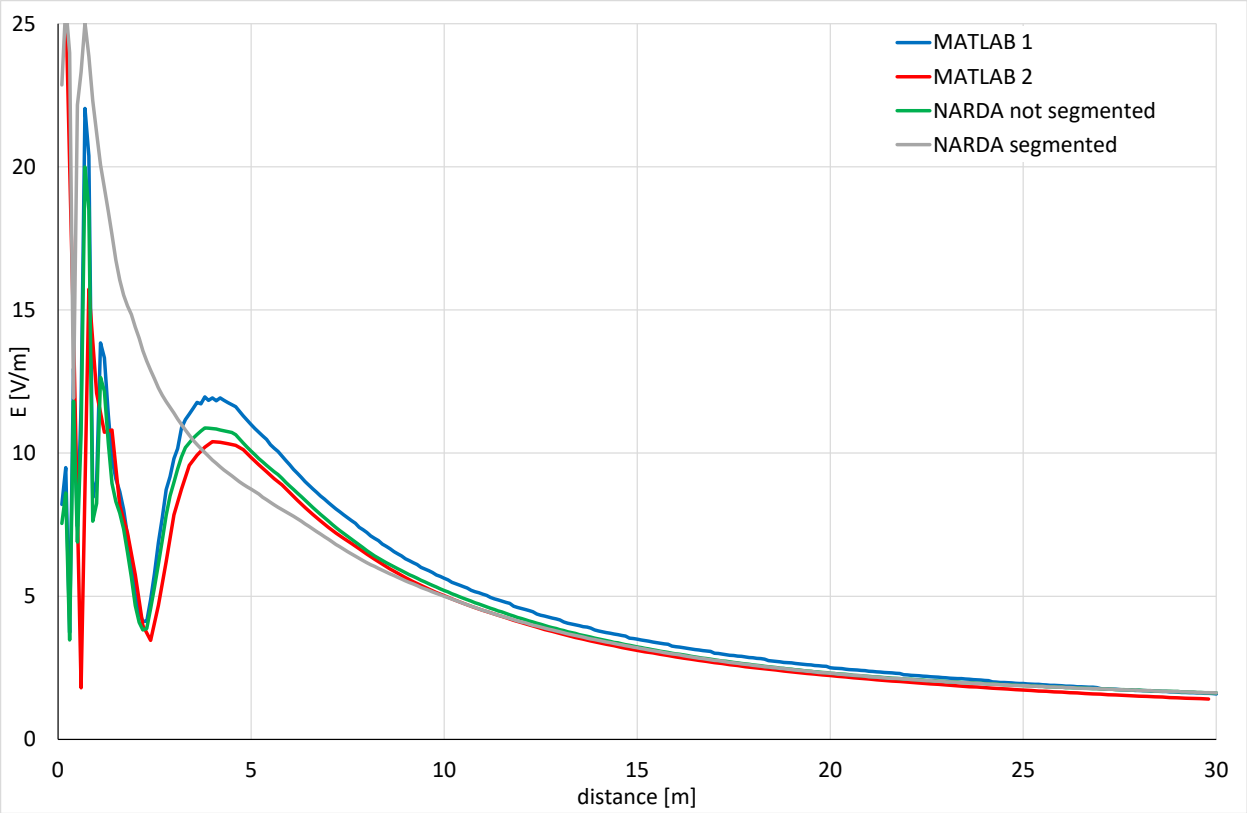

Figure 5. Electric field for open space common scenario for different models (MATLAB 1 = phasor sum, MATLAB 2 = power sum).

Table 1. Maximum, 95th percentile, average, median and standard deviation of the electric field [V/m] for open space common scenario for different models.

	MATLAB 1	MATLAB 2	NARDA not segmented	NARDA segmented	(max - min) / avg
Max	26.00	26.78	23.72	46.25	0.73
E95	9.43	8.36	8.66	8.43	0.12
AVG	4.27	3.80	3.93	4.11	0.12
E50	2.52	2.23	2.32	2.31	0.12
STD	5.59	5.14	5.11	6.30	0.21

The last column in Table 1 represents the maximum normalized difference between each result. It is calculated as the difference between maximum and minimum value of each statistic divided by the average value of each statistic. For all important parameters it is 0.12.

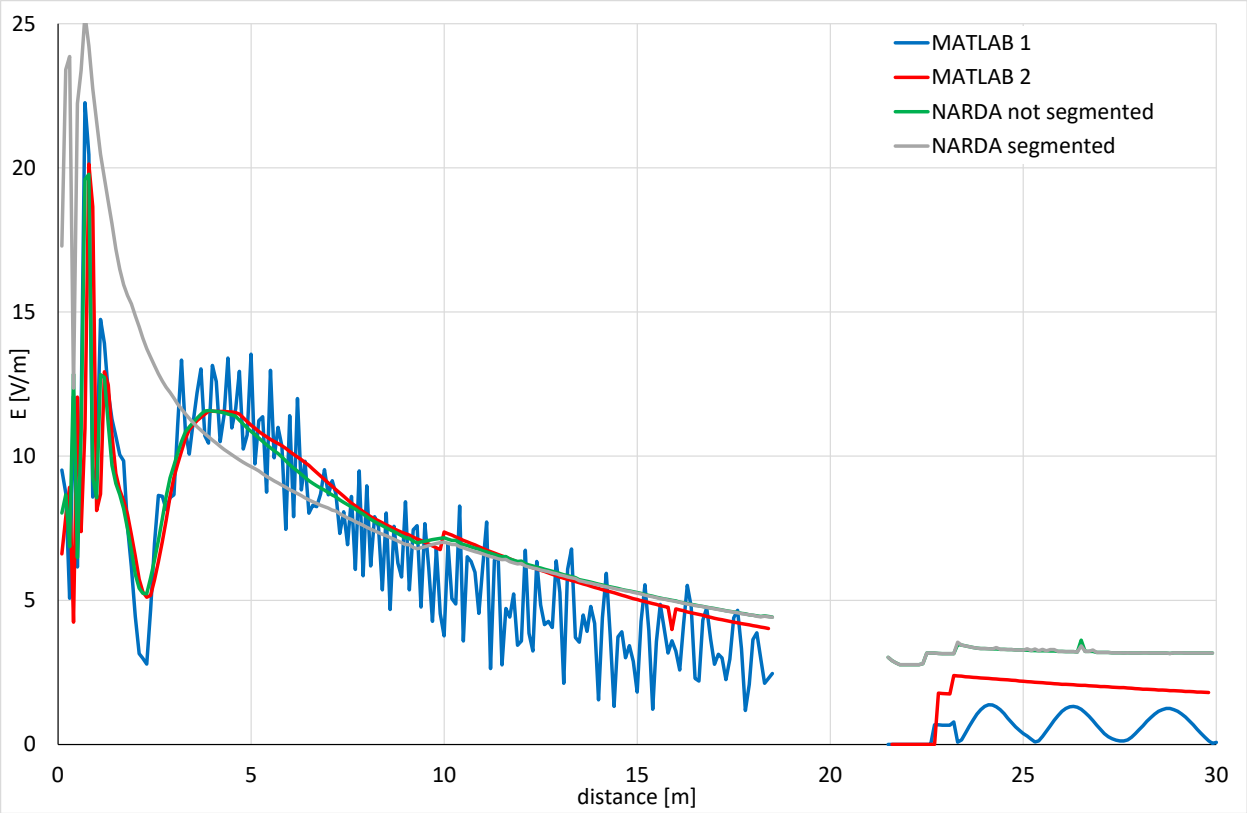

Figure 6. Electric field for cluttered common scenario for different models (MATLAB 1 = phasor sum, MATLAB 2 = power sum).

Table 2. Maximum, 95th percentile, average, median and standard deviation of the electric field [V/m] for cluttered common scenario for different models.

	MATLAB 1	MATLAB 2	NARDA not segmented	NARDA segmented	(max - min) / avg
Max	26.55	23.82	23.71	50.48	0.86
E95	9.74	9.96	9.85	9.81	0.02
AVG	4.18	4.66	4.99	5.15	0.20
E50	1.72	2.69	3.31	3.30	0.58
STD	5.99	5.90	5.66	6.71	0.17

Similar trends were obtained also for cluttered common scenario presented in Figure 6 and Table 2. There, the MATLAB 1 calculation took into account the phase of rays, whereas other calculations did not consider phase of rays. As it can be seen from results in Table 2, this does not influence the statistical results except the maximum value, which can be expected.

The last column in Table 2 represents the maximum normalized difference between each result. It is calculated as the difference between maximum and minimum value of each statistic divided by the average value of each statistic. For 95th percentile the difference is only 0.2, whereas or the average value it is 0.2 and for median value it is 0.58.

Based on the comparison of all statistical results we conclude that both numerical tools are suitable for numerical calculations of indoor and outdoor exposure scenarios. There is no significant difference between the results of calculations with resolution of 0.1 m and 0.3 m and although the model with the phase gives slightly different local distribution of electric field due to interferences between all rays, the statistical values are not influenced by the omission of phase in the calculations.

3 Numerical estimation of exposure to RF EMF in Industry 4.0 applications

This section has as objective to determine relevant RF EMF exposure scenarios, to adapt in-house tools to simulate these scenarios, to compare simulations of the different partners, and lay a foundation for validation with real on-site measurements in D2.3.

Exposure is estimated by simulating the propagation of RF EMF in various industrial environments. The different software tools used require the user to recreate the 3D propagation environment at a certain level of detail and specify the location of the transmitter and receiver. The output of the software can be a set of propagating plane waves ('multipath components', MPCs) between the transmitter and receiver. A worker's exposure to the local network is determined by the electric (E) fields in the FR1 band or incident power densities (S) in the FR2 band.

3.1 Exposure simulation scenarios

This subsection describes the different relevant scenarios that were simulated by the different partners. To validate the different methods and software used by the partners, we start off with a common scenario that is simulated by INIS, AUTH and IMEC, to assess if the different partners obtain the same or similar results. Then, seven more scenarios are described. Simulations results are then presented in Section 2.2.

3.1.1 FR1: 3.6 GHz – indoor smart Industry 4.0

For the smart Industry 4.0 scenario, two environments are analyzed. In both environments a private standalone (SA) 5G network is installed using the same radio equipment. One environment is a warehouse and the second is a production hall in one of the smart industry facilities of a key global leader in smart IoT solutions.

The private network operates in the medium band of the 5G frequency spectrum, namely, band n78, and its frequency range is from 3700 to 3800 MHz for industrial use (100 MHz bandwidth). For the indoor network, Nokia's AirScale AWHQB pRRHs serve as small cell access points with a maximum power of 1 W. These are connected at every relevant location in the warehouse and the production building with an ASiR hub with a direct optic fiber connection to the baseband unit (BBU) and the core server in the central data center. The radiation pattern of the pRRHs is nearly isotropic, with antenna gain of 0 dBi. The network's time division duplex (TDD) ratio, indicating the maximum time portion during which the network operates in downlink mode, is 0.6.

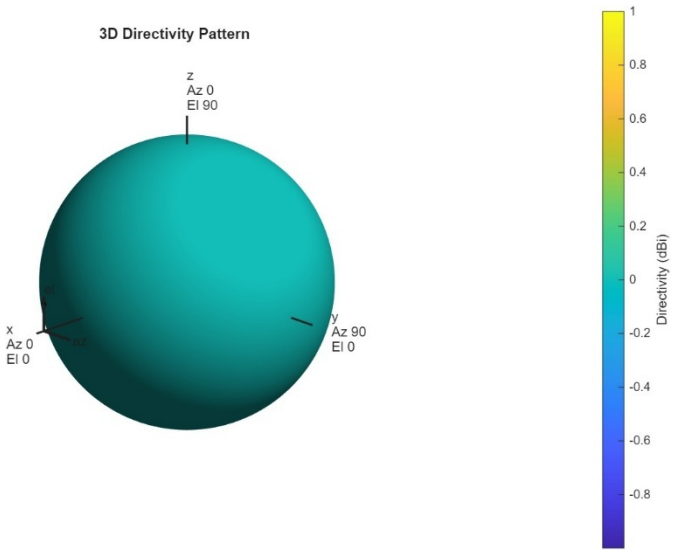

Figure 7. 3D directivity pattern of modelled antenna (Nokia's AirScale AWHQB)

Also, both environments share the same basic characteristics. Both have a concrete floor, the walls are made mostly of concrete, and the roof is made of trapezoidal corrugated metal.

3.1.1.1 Warehouse Germany

The industrial private network under test is composed of 4 pRRHs spread over the entire warehouse building. pRRHs were mounted under the roof at a height of about 5 m.

The warehouse building covers an area of 3399 m^2, and its height is 5.5 m. The warehouse is mainly used for storing reprocessing material, other necessary components and final products, high-tech digital structures, and circuits. There are two offices inside the warehouse; the offices are made of metallic walls with large windows. The offices extend up to the ceiling, and the racks' top shelves are located close to the ceiling so that when they are full, stored items nearly reach the ceiling. The pallet racks are 1 m deep, with the exception of the first (lowest) rack, which is wider, with very narrow passages between. The racks and offices cover about 40 % of the warehouse's area. The detailed geometry of the warehouse is shown in Figures 8 and 9.

This warehouse environment was calculated with NARDA and by MATLAB, only NARDA results will be presented.

Figure 8. Geometry for the warehouse in Germany. Black lines represent the walls, dark grey blocks are pallet racks, and light grey blocks are the offices. Locations of the pRRHs are indicated with 'RH'.

Figure 9. Detailed geometry of pallet racks modelled in Blender Ver 4.4 for MATLAB simulations. Wooden pallets carrying chipboard boxes of different sizes are arranged on metal frames.

Table 3: base station technical parameters for warehouse Germany scenario

Location description	
type of location	logistics - warehouse
type of installation	private operational site
Antenna parameters	
antenna model	4 pico indoor remote radioheads Nokia AirScale SiR-pRRH AWHQB
antenna type	omnidirectional
antenna gain [dBi]	0
location of antenna	under ceiling
antenna height (middle) [m]	5
antenna size [m]	≈0.3
downtilt [°]	0
envelope of radiation pattern in use	only one radiation pattern, no beamforming
Cell parameters	
Type	5G
frequency band	3.5 GHz
central frequency [MHz]	3750
channel number (center)	650000
bandwidth [MHz]	100
MIMO configuration	4×4
max output power [W]	4×0.25
max output power [dBm]	4×24 dBm
duty cycle	0.6
power of pilot signal [dBm]	-11.15
frequency of the pilot [MHz]	3748
pilot channel number	649920
PCI	606
sub carrier spacing (SCS) [kHz]	30

3.1.1.2 Production hall

The production hall is covered by 6 pRRHs. Four of them are mounted on the roof beams at a height of about 5.9 m, whereas two of them are mounted under the balcony at a height of 3.1 m.

The production building, which is attached to the warehouse, covers an area of about 2800 m^2, and its height is 6.9 m. The majority of the production building is occupied by a production hall with a surface of 2117 m^2. The remainder of the building is occupied by two-level offices, with a balcony on the first floor running at a height of 3.4 m, extending inside of the production hall.

Inside the hall there are several dedicated working places for different tasks, mainly for assembly and testing, which are grouped into 4 production areas with 4 corridors between. The production areas cover about 35 % of the total area of the production building and 46 % of the production hall. However, because the production facilities cover only a portion of the production area, the effective equipment coverage of the production hall is below 20 %. All equipment is relatively low, with the tallest items not exceeding 2.5 m. The detailed geometry of the production hall is shown in Figures 10 and 11. The technical parameters of the base station are listed in Table 4. The production hall environment was calculated with NARDA.

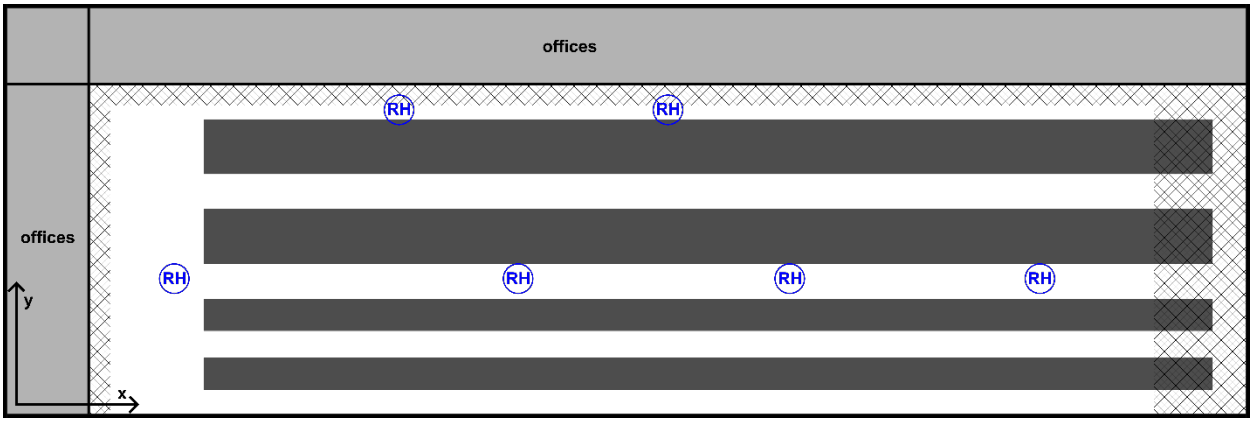

Figure 10: Geometry for the production hall. Black lines represent the walls, dark grey blocks are pallet racks, light grey blocks are the offices, and the grid pattern is the balcony. Locations of the pRRHs are indicated with 'RH'.

Figure 11: Locations of pRRHs inside of the production hall (blue dots).

Table 4: base station technical parameters for production hall scenario

Location description	
type of location	production facility
type of installation	private operational site
Antenna parameters	
antenna model	5 pico indoor remote radioheads Nokia AirScale SiR-pRRH AWHQB
antenna type	omnidirectional
antenna gain [dBi]	0
location of antenna	4 under ceiling and 2 under balcony
antenna height (middle) [m]	5.9 and 3.1
antenna size [m]	≈0.3
downtilt [°]	0
envelope of radiation pattern in use	only one radiation pattern, no beamforming
Cell parameters	
type	5G
frequency band	3.5 GHz
central frequency [MHz]	3750
channel number (center)	650000
bandwidth [MHz]	100
MIMO configuration	4×4
max output power [W]	4×0.25
max output power [dBm]	4×24 dBm
duty cycle	0.6
power of pilot signal [dBm]	-11.15
frequency of the pilot [MHz]	3748
pilot channel number	649920
PCI	607
sub carrier spacing (SCS) [kHz]	30

3.1.1.3 Parametric study of clutter attenuation

A parametric study was conducted to determine the value of the attenuation of the pallet racks that gave the most accurate results compared to the measurements. The value of the reflection coefficient of the pallet racks varied from 2 dB to 5 dB, with an additional value of 100 dB representing the case of infinite attenuation of pallet racks. Results of all calculations at the measurement locations (Figure 8) were compared to the results of measurements. Several statistical metrics were calculated to determine the most accurate value of the reflection coefficient:

- Relative error of the 95th and 50th percentiles of the electric field; the closer the value of both percentiles for the calculated and measured results, the more accurate the value of the reflection coefficient. The 95th and 50th percentiles of the electric field were determined by first squaring all results, calculating the percentile value of squares, and, finally, rooting the percentile value.

- Root mean square error, normalized root mean square error, and root mean square relative error of the calculated electric field compared to the measured electric field; square errors are more appropriate than linear errors, as the exposure is related to the square of the electric field. The lower the errors, the better the agreement of both results.
- Pearson correlation coefficient r; the higher the number of the r parameter, the better the correlation of the calculated data with the measured data. The Pearson correlation coefficient was calculated for the square of the electric field.
- Kolmogorov–Smirnov (K-S) test; the Kolmogorov–Smirnov test gives information about the similarity of two distributions. All previous metrics compare results point to point. However, in the complex indoor environment, there are many variables and factors affecting detailed electric field distribution that are not possible to include in a model. This means that calculated results and measured results can differ significantly if compared point to point, but the overall exposure is still very similar, because maybe the model predicted one hotspot at a certain location, but, in reality, it was positioned on some other location. Therefore, important information when comparing two datasets of results that represent the exposure is the similarity of the distributions of both datasets. The smaller the value of the Kolmogorov–Smirnov test, the more similar the distributions of both results.

The analysis presented in Table 5 confirms that 3 dB attenuation delivered the best overall performance across all evaluation metrics. It achieved the lowest error for the 50th percentile (E50), the smallest root mean square and normalized root mean square errors, and optimal distributional match (lowest K-S statistic). While ranking second for 95th percentile (E95) estimation and third for Pearson correlation coefficient (r = 0.893), its correlation performance remained nearly identical to the top result (0.895). Importantly, this 3 dB value consistently ranked among the top two performers for all statistical measures evaluated, demonstrating the best trade-off between under- and over-estimation across corridors with varying clutter densities. Given the practical need for a single representative attenuation value, 3 dB provided the smallest average error, the strongest distributional similarity, and robust correlation, making it the most balanced and reliable selection for comprehensive modeling.

Therefore, for further numerical modeling, the attenuation of 3 dB was selected for pallet racks in Narda EFC 400 models.

Table 5. Results of the parametric study of the attenuation of the pallet racks. Results of calculations at the measurement locations (Figure 8) were compared to the results of measurements. For each analyzed parameter, the best result is highlighted in green, and the second best is highlighted in blue. For the K-S test, results are compliant if the value is below 0.21.

Attenuation of Pallet Racks [dB]	E95	E50	Root Mean Square Error [V/m]	Normalized Root Mean Square Error	Root Mean Square Relative Error	Pearson Correlation Coefficient r	Pearson Correlation Coefficient p	K-S Test
2 dB	−0.029	0.048	0.141	0.259	0.446	0.887	0.000	0.13
3 dB	−0.034	−0.051	0.134	0.247	0.327	0.893	0.000	0.10
4 dB	−0.036	−0.157	0.139	0.255	0.302	0.895	0.000	0.13
5 dB	−0.037	−0.265	0.147	0.270	0.320	0.895	0.000	0.18
100 dB	−0.041	−0.499	0.201	0.369	0.573	0.905	0.000	0.33

For the MATLAB simulations, the pallet racks were modeled as wooden pallets carrying chipboard boxes of various sizes arranged on metallic frames (see Figure 9). The racks were mostly filled, with only about 10 to 20 % of the volume remaining empty. Because the MATLAB tool does not account for transmission through objects, it was assumed that the partial transmittance through the racks was proportional to the percentage of empty space. Based on this assumption, the effective attenuation introduced by the pallet racks was estimated to be between 14 and 20 dB.

3.1.2 FR1: 3.5 GHz – Port of Koper, outdoor macro cell

In Port of Koper, Slovenia two 5G deployment scenarios were assessed. First scenario was installation of private standalone 5G network operating at 3.5 GHz, which served for the common scenario. Second scenario was based on a private slice in the existing public 3.5 GHz 5G network. This scenario is based on a private slice, that uses only base stations located inside the area of Port of Koper. The scenario includes one such base station, mounted on a pole, located in the corner of big car parking garage (see Figure 12).

Figure 12. Locations of base station at the corner of the parking garage.

The base station used for private slice is a public 5G base station operating at the central frequency of 3470 MHz and with the bandwidth of 100 MHz. The radio head is Ericsson AIR 3227, which is a beamforming unit with an 8x8 configuration. It has a maximum output power of 100 W and a duty cycle of 0.8 and a maximum gain of 23.5 dBi. Its directivity pattern is presented in Figure 13.

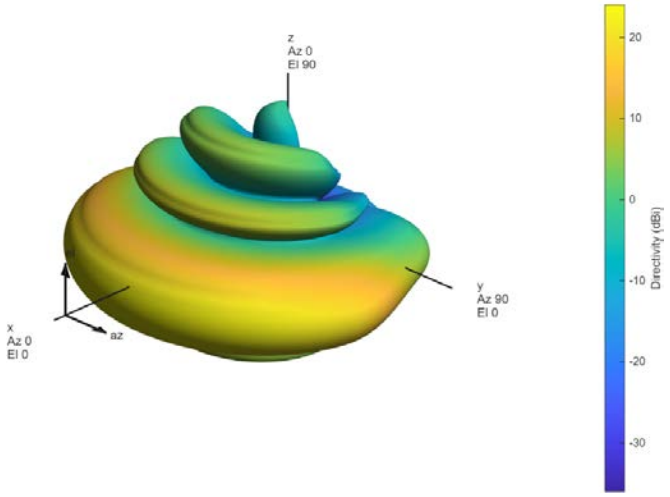

Figure 13. 3D directivity pattern of modelled antenna (Ericsson AIR 3227)

The antenna is mounted on the pole at a height of 9.2 m above the level of the top parking lot. This public 5G base station with private slice scenario was calculated with NARDA. The technical parameters of the base station are listed in Table 6:

Table 6. Base station technical parameters for Port of Koper scenario

Location description	
type of location	logistics - Port
type of installation	public site with test private slice
Antenna parameters	
antenna model	Ericsson AIR 3227
antenna type	directional
antenna gain [dBi]	23.5
location of antenna	on pole
antenna height (middle) [m]	9.2
antenna size [m]	0.54
downtilt [°]	0
envelope of radiation pattern in use	beamforming
Cell parameters	
type	5G
frequency band	3.5 GHz
central frequency [MHz]	3470
channel number (center)	631333
bandwidth [MHz]	100
MIMO configuration	8×8
max output power [W]	100
max output power [dBm]	50
duty cycle	0.8
power of pilot signal [dBm]	/
frequency of the pilot [MHz]	3430.56
pilot channel number	628704
PCI	261
sub carrier spacing (SCS) [kHz]	30

3.1.3 FR1: 3.5 GHz – Office, pico cell

In an office hall private 5G network is installed. The hall covers the area of about 400 m^2 and is made mostly of concrete; the metal roof is at the height of 7 m. On one side of the hall there are about 6 m wide metal doors covering the entire height of the wall. One side of the hall borders with additional offices, this side is covered with metallic plates and it has some small windows. There are no high items in the hall. Figure 14 shows the layout of the considered environment.

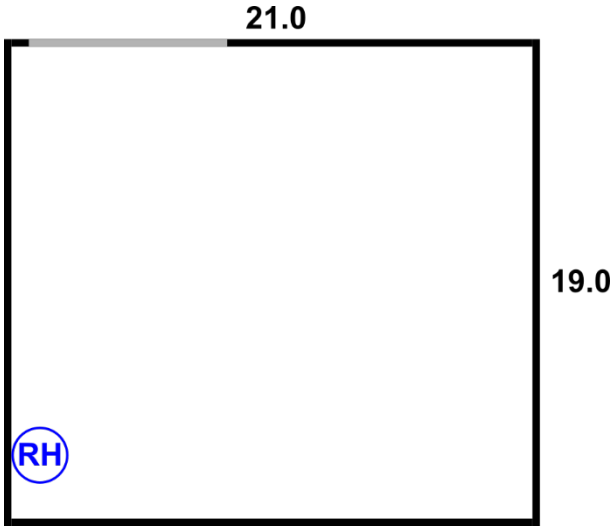

Figure 14. Geometry of the test hall. Black blocks represent the walls and grey block are doors. 'RH' represents the location of the antenna. (dimensions in m)

The private SA 5G network operates in the frequency range of 3420 to 3520 MHz. The Ericsson 6524 antenna with a gain of 12 dBi is mounted on the wall at the height of 3 m, the size of the antenna is 0.2×0.2 m. Configuration is 4×4 with a power of 4×5 W, corresponding to a total power delivered to the antenna of 20 W. The duty cycle is 0.8. The antenna's directivity pattern is presented in Figure 15. The technical parameters of the base station are listed in Table 7. The office scenario was calculated with NARDA and MATLAB, only NARDA results will be presented.

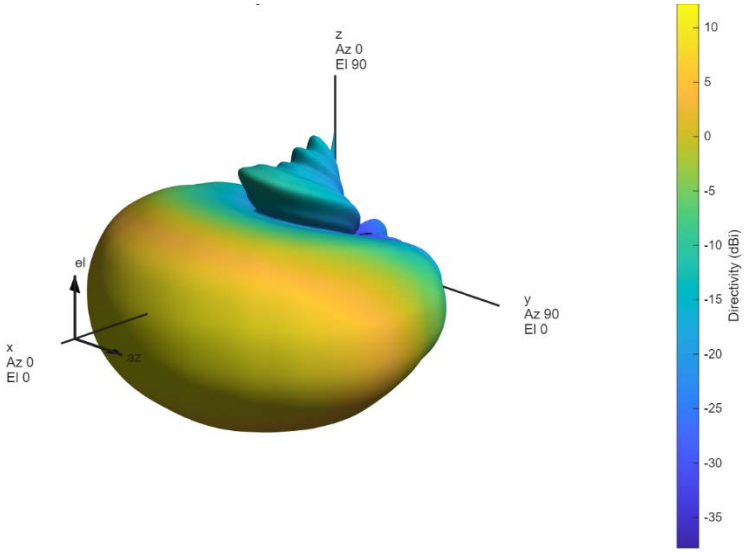

Figure 15. 3D directivity pattern of modelled antenna (Ericsson 6524)

Table 7. Base station technical parameters for office pico cell scenario

Location description	
type of location	test facility
type of installation	private operational site
Antenna parameters	
antenna model	Ericsson 6524
antenna type	directional
antenna gain [dBi]	12
location of antenna	on the wall
antenna height (middle) [m]	3
antenna size [m]	≈0.2×0.2
downtilt [°]	0
envelope of radiation pattern in use	only one radiation pattern, no beamforming
Cell parameters	
type	5G
frequency band	3.5 GHz
central frequency [MHz]	3470
channel number (center)	631333
bandwidth [MHz]	100
MIMO configuration	4×4
max output power [W]	4×5
max output power [dBm]	4×24 dBm
duty cycle	0.8
power of pilot signal [dBm]	/
frequency of the pilot [MHz]	3430.545
pilot channel number	628703
PCI	275
sub carrier spacing (SCS) [kHz]	30

3.1.4 FR1: 3.5 GHz – Warehouse Belgium

For this scenario, we consider a test factory with an existing 4G/5G deployment. The factory is an industrial environment in Ghent, Belgium, with 6 rows of racks, see Figure 16. Outer walls are made of concrete. The middle four rack rows consist of two racks next to each other, leading to a total of 10 racks in the area. At 6 locations in the area, which measures 74 x 36 m², collocated 4G/5G base stations are mounted, operating at a frequency of 2600 and 3500 MHz respectively. Figure 16 (left) shows the ground plan of the environment (racks in red, BS in green) and a picture of the (empty) metal racks (right). The 4G network uses two-sector antennas with a 7.5 dBi gain and horizontal and vertical beamwidths of 71 and 72° respectively. The 5G antennas are also two-sector antennas with a 7.7 dBi gain and horizontal and vertical beamwidths of 68 and 69° respectively.

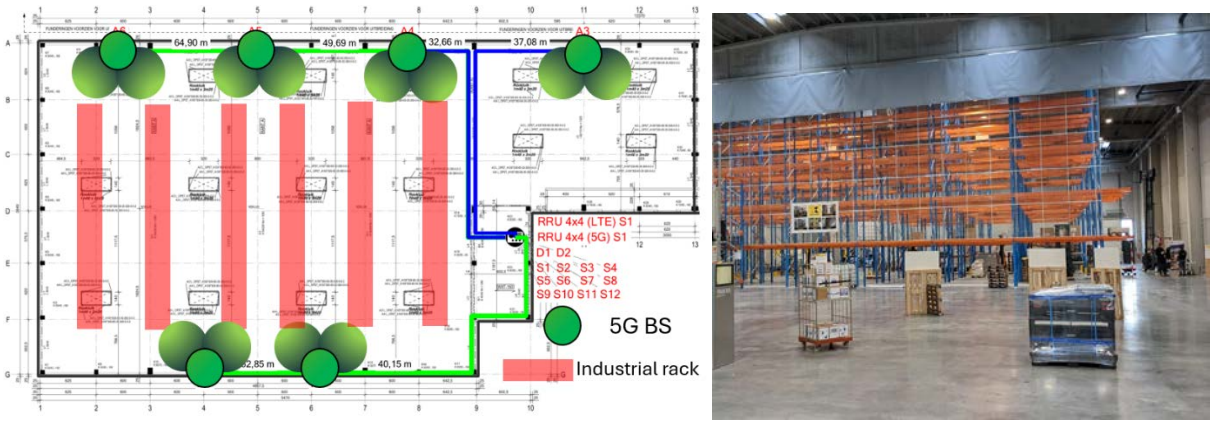

Figure 16. Ground plan of the realistic simulated industrial environment (left; racks in red, BS in green) and a picture of the (empty) metal racks (right)

The proposed simulations were executed based on this actual deployment, containing metal racks, and equipped with six 4G/5G base stations, operating at 2.6 and 3.5 GHz respectively, with a 43 dBm EIRP per BS, assuming an omnidirectional radiation pattern. The antenna's directivity pattern is presented in Figure 17.

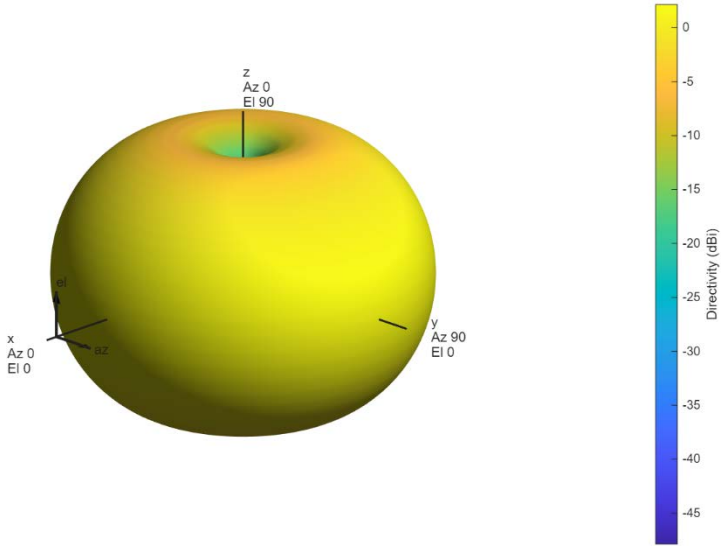

Figure 17. 3D directivity pattern of modelled antenna

As propagation model, we assumed free-space propagation with added rack losses, for cases where the direct ray between BS and receiver point intersects with the rack. This follows a similar approach as a multiwall path loss model where wall losses are cumulated and added to free-space losses. Rack height is 600 cm, base station height is 800 cm, receiver height is 130 cm. A single rack was assumed to cause a 2.3 dB loss, a double rack 4.6 dB. We assumed a worst-case 100% downlink duty cycle with all sources active. Given the large beamwidth of the two sectors,

we assume an omnidirectional pattern with maximal gain for the simulations. The technical parameters of the base station are listed in Table 8. This simulation was conducted with the WHIPP tool.

Table 8. base station technical parameters for FR1 warehouse Belgium scenario

Location description	
type of location	warehouse – factory
type of installation	private test site
Antenna parameters	
antenna model	CMAX-DMF4-43-WI53
antenna type	directional
antenna gain [dBi]	7.7 at 2600 – 7.8 at 3500
location of antenna	on wall
antenna height (middle) [m]	8
antenna size [m]	0.33 x 0.46 x 0.1 m
downtilt [°]	0
envelope of radiation pattern in use	Antennas approximated as omnidirectional towards users
Cell parameters	
type	4G-5G
central frequency [MHz]	2600-3500 GHz
MIMO configuration	4x4 for 5G at 3500 GHz
output power [dBm]	43 dBm
duty cycle	1

3.1.5 WiFi 6: 5.5 GHz – Lab scenario, beamforming

In this scenario, we examined the exposure of workers inside a laboratory due to a wireless local area network (WLAN). WLANs are commonly used in modern work environments, enabling seamless communication, collaboration, and productivity among employees who utilize a variety of connected devices, many of which may not be compatible with wired infrastructure. WLAN technology has evolved to incorporate advanced features such as antenna beam steering and operation at higher radio frequencies, which support faster data rates and wider coverage. These developments also influence the temporal variation of exposure to radiofrequency electromagnetic fields (RF-EMF) in the workplace. Wi-Fi 6, or IEEE 802.11ax, is an IEEE standard for WLANs that operates in the 2.4 GHz and 5 GHz bands and employs beamforming to steer the signal to a specific user rather than broadcasting it in all directions. A comparison of the exposure levels was made when the radiation pattern of the transmitting antenna system is static and when beamforming is used.

3.1.5.1 Environment

Figure 18 shows the environment in which the exposure was assessed: a laboratory within the premises of the Aristotle University of Thessaloniki, Greece covering an area of approximately 63 square meters. Within this space, five workstations are situated along the windows which span two sides of the room. The AP is centrally located on the ceiling, at a height of 2.8 m. The 3D

model of the site was created with Blender software (https://www.blender.org/) and includes the ceiling, walls, floor, windows, desks, drawers, cabinets and some laboratory equipment.

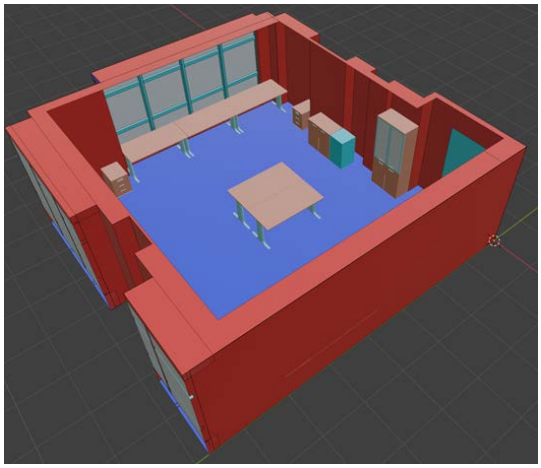

Figure 18: 3D representation of the laboratory at AUTH. The ceiling is omitted to enhance visibility. Colors indicate different material types

3.1.5.2 Transmitter

Figure 19 shows the transmitter, a WiFi-6 Cisco Catalyst 9115 enterprise access point operating at 2.4 and 5 GHz frequency bands with a maximum transmit power of 23 dBm. The antenna system is comprised of four dual-band dipoles (Cisco AIR-ANT2524Dx-Rx Series) mounted at the vertices of a square with side 12.4 cm. The maximum directivity of each dipole is 4 dBi at the 5 GHz band and its antenna pattern is provided by the manufacturer (Figure 19c).

(a) (b) (c)

Figure 19: Transmitter. a) WiFi-6 access point without the dipole antennas. b) Dipole antenna. c) Azimuth and elevation plane radiation pattern of the dipole antenna

For our simulations we used the AP's geometry and the dipole's radiation pattern to model the entire antenna system in Matlab, as a 2x2 Uniform Rectangular Array, as shown in Figure 20. The magnitude and phase of the four antenna elements are adjustable, allowing the radiation pattern to be dynamically modified and steered to form a high-gain beam toward a specific location. The operating frequency was set to 5.5 GHz, and the transmit power was 23 dBm, which is the

maximum output power of the access point according to the manufacturer. The technical parameters of the transmitter are listed in Table 9.

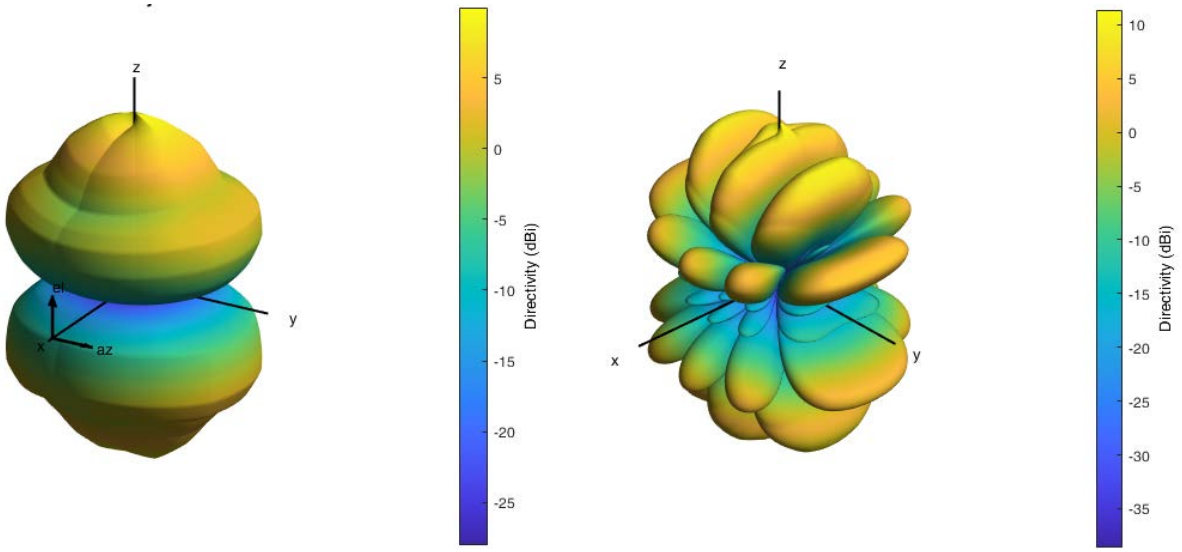

(a) (b)

Figure 20. Modeled transmitter: (a) 3D directivity pattern of a single dipole antenna. (b) 3D directivity pattern of the antenna array

Table 9. Base station technical parameters for WiFi lab scenario

Location description	
type of location	Laboratory
type of installation	private operational site
AP's antenna parameters	
AP model	Cisco Catalyst 9115
antenna type	4 element array
antenna gain [dBi]	4 per antenna element
location of antenna	on the ceiling
antenna height (middle) [m]	2.8
antenna size [m]	≈0.124×0.124×0.16
downtilt [°]	0
envelope of radiation pattern in use	Beamforming
Transmission parameters	
Type	Wi-Fi 6
frequency band	5 GHz
central frequency [MHz]	5.5
channel number (center)	100
bandwidth [MHz]	20
MIMO configuration	2×2
max output power [W]	0.2
max output power [dBm]	23
duty cycle	1

3.1.5.3 Exposure assessment calculations

In the simulation, the MATLAB ray tracing tool using phasor sum was used, where each ray was limited to a maximum of two reflections and one diffraction. The angular separation of the shooting rays was approximately 0.5 degrees. In cases where beam steering was employed, the direction of the user was determined by identifying the ray with the lowest path loss. Using the angle of departure of that ray, a steering vector was calculated and applied to the elements of the transmitter's antenna array, resulting in a high-gain beam directed toward the user.

3.1.5.4 Simulation scenarios

Three simulation scenarios were examined, focusing on the effects of beamforming on the exposure of users and bystanders compared to a static radiation pattern. In all scenarios, the worst-case exposure was considered, with the transmitter operating at its maximum power and a 100% duty cycle. The electric field was evaluated at a height of 1.1 m in all cases. The three scenarios differ in the number and location of users and non-users (bystanders) of the network.

1. *Exposure on workstation positions*

For the first simulation scenario, we assessed the maximum EMF exposure at the positions of the five laboratory workstations (A to E in Figure 21). These positions represent typical locations where users are seated and operating wireless devices within the lab environment. Initially, we calculated the electric field using a static radiation pattern for the transmitter, in which all antenna array elements were configured with equal amplitude and phase. This configuration simulates a uniform, non-directional transmission, providing a reference case for comparison.

Subsequently, we introduced beamforming by assuming that all wireless network traffic originated from user terminals located at positions A to E, one at a time. In each case, the system directed a high-gain beam toward the active user location by dynamically adjusting the amplitude and phase of the antenna array elements. The beam was steered sequentially to each workstation, in order to evaluate how beamforming affects EMF exposure at each position compared to the static case.

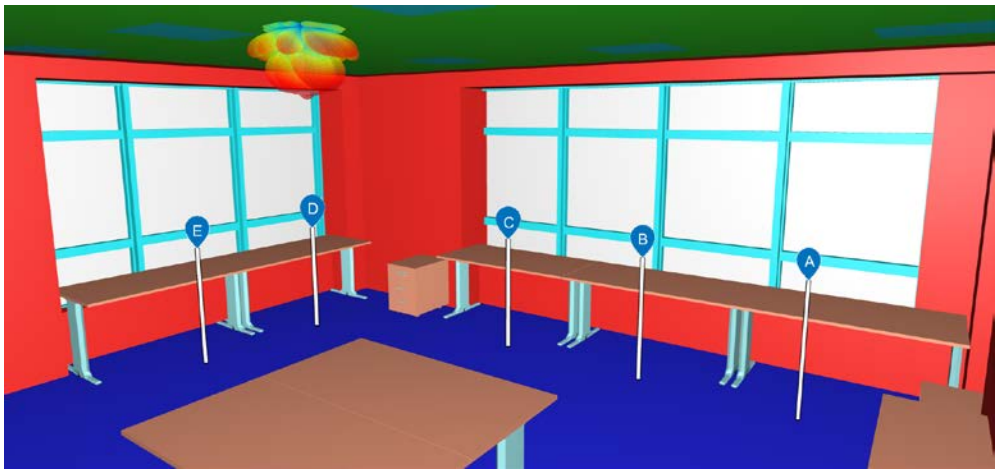

Figure 21. Locations of the transmitter and five workstations.

2. Exposure on moving active user and workstations

For the second simulation scenario, we again considered the five workstation positions from Scenario 1 (A to E). In this case, however, we assumed that a single active user, responsible for generating all traffic in the wireless network, was initially located at position B and then moved across the laboratory toward the exit door, as shown in Figure 22. As the user moved, the transmitter continuously steered a high-gain beam toward their position by dynamically adjusting the antenna array's phase and amplitude. To simulate the user's movement, the path from position B to the door was divided into 34 discrete steps, representing different user positions along the route. At each step, the electric field was calculated at the user's location to evaluate the variation in exposure during movement. Additionally, for each step of the active user's movement, we also calculated the incident electric field at the fixed positions A, C, D, and E, where bystanders are assumed to be located.

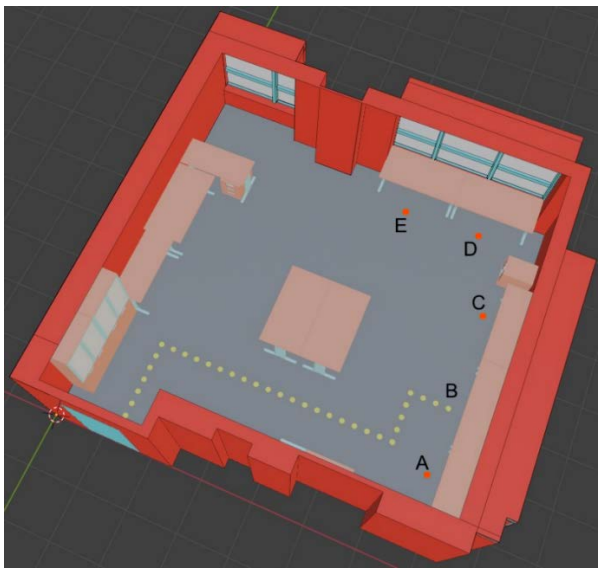

Figure 22. Positions of active user (yellow dots) and bystanders (red dots)

3. Generalized exposure assessment

For the final simulation scenario, we examined the exposure of users and bystanders not at specific, predefined locations, but across the entire laboratory space for a more generalized and comprehensive approach. To this end, we randomly selected 101 spatial positions within the laboratory, which represents a relatively high spatial sampling density given the lab's overall size. Positions occupied by furniture or equipment were excluded, restricting the selected points to areas of free space where personnel could realistically be present.

We first calculated the electric field at all 101 positions using a static radiation pattern, where the antenna array radiates uniformly in all directions. Next, for the beamforming case, we sequentially steered a high-gain beam toward each of the 101 positions, treating each one as an active user position. For each of these beam-steering instances, we calculated the electric field at the active user's location (the beam target), as well as at the remaining 100 positions, which are treated as bystander locations for that instance. To expand the datasets, particularly the E-field values obtained with the static radiation pattern as well as the user's E-field values with the beamsteering radiation pattern, we repeated the simulations with different random points 10 times.

As a result, we generated a dataset consisting of: 1010 electric-field values for the static radiation pattern case, 1010 electric-field values at the active user positions under beamforming, and 101000 (100 × 101 × 10) values representing bystander exposure in the beamforming case. This scenario allows for a statistical evaluation of exposure variation throughout the environment under both static and beamsteered conditions.

3.1.6 FR2: 26 GHz – Lab scenario, beamforming

In a research facility, a private test 5G network was installed in an anechoic chamber, as shown in Figure 23. The size of the anechoic chamber is 12 m × 12 m. The private SA 5G network operated in the frequency range of 25.5-25.9 GHz using the bandwidth of 4 × 100 MHz. The Nokia AWEUC AirScale radio head with active beamforming had a gain of 27 dBi and was mounted on the movable pole at a height of 1.5 m, the size of the antenna was about 0.2×0.2 m. The MIMO configuration was 2×2 and the power delivered to antenna was 1 W. Duty cycle was 0.8. The antenna's directivity pattern is presented in Figure 24. The technical parameters of the base station are listed in Table 10. This lab scenario was calculated with NARDA.

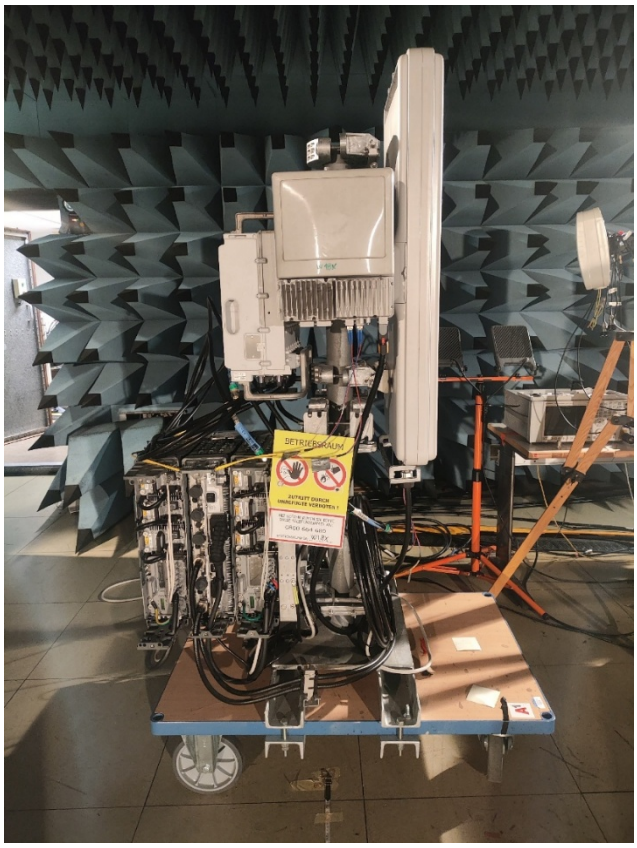

Figure 23. Location of the equipment under test.

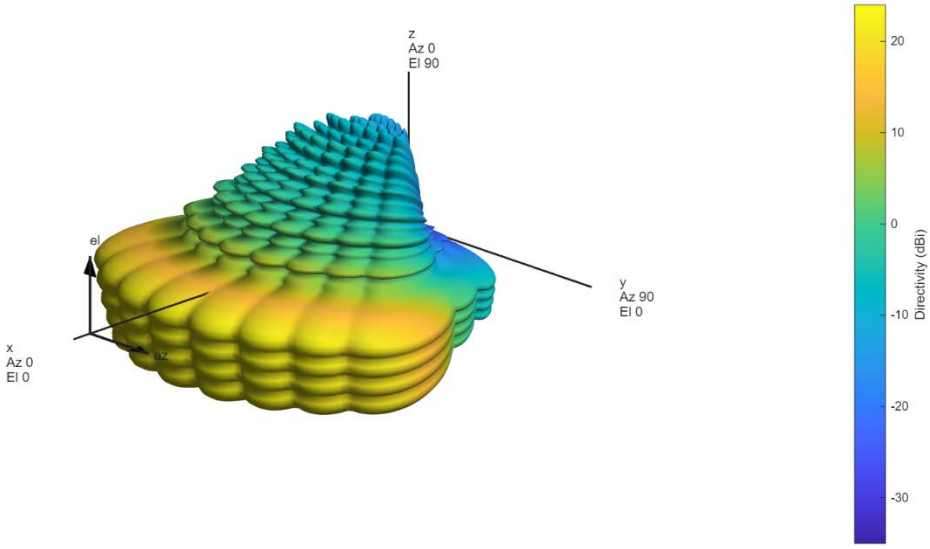

Figure 24. 3D directivity pattern of modelled antenna

Table 10: base station technical parameters for FR2 lab scenario

Location description	
type of location	test installation in anechoic chamber
type of installation	private test site
Antenna parameters	
antenna model	Nokia AWEUC AirScale
antenna type	directional, vertical polarization
antenna gain [dBi]	27
location of antenna	on the pole
antenna height (middle) [m]	1.5
antenna size [m]	≈0.2×0.2
downtilt [°]	0
envelope of radiation pattern in use	two scenarios, one directional high gain with beamforming, one wide with no beamforming
Cell parameters	
type	5G
frequency band	26 GHz
central frequency [MHz]	25700
channel number (center)	2040832
bandwidth [MHz]	400 (4 × 100)
MIMO configuration	2×2
max output power [W]	1
max output power [dBm]	30
duty cycle	0.8
power of pilot signal [dBm]	/
frequency of the pilot [MHz]	25563.36
pilot channel number	2038555
PCI	/
sub carrier spacing (SCS) [kHz]	240
Measurement conditions	
type of measurements	band selective measurements

3.1.7 FR2: 28 GHz – Warehouse Belgium, beamforming

This scenario specifically investigated exposure of users and non-users in 5G mmWave communication in an industrial environment. The demand for higher data rates in 5G has necessitated deployments at higher frequencies, specifically in the Frequency Range 2 (FR2) range from 26 GHz to 71 GHz, which offers greater bandwidth but also results in higher Path Loss (PL). This requires a denser network of Base Stations (BSs), positioned closer to users to maintain service quality and network coverage. To counteract the rapid signal attenuation associated with these higher frequencies and enhance signal transmission efficiency, the adoption of directional beams through massive MIMO arrays has been proposed. While this technology effectively concentrates energy within the antennas' beams, it concurrently increases RF-EF exposure for users. Currently, exposure research in the FR2 band, particularly around 28 GHz, is limited, e.g., [Shikantsov]. Therefore, this simulation aimed to evaluate RF-EF exposure using beamsteering massive MIMO technologies in a realistic 2600m² industrial warehouse with metal racks

containing different materials, and equipped with 5G at the 28 GHz band. We analyzed both user and non-user exposure levels for different MIMO array sizes, and determined spatial and spatiotemporal duty cycles.

3.1.7.1 Environment

Figure 25 depicts the industrial **environment** in "Fabriek Logistiek" of 74x36 m in Ghent, Belgium. This area is 10 m high, with outer walls made of concrete. The building contains 10 metal industrial racks (8 m high) uniformly distributed throughout the space. Here, we analyzed the racks empty or filled with a mixture of three materials: metal, wood, and plastic tanks containing water. The electromagnetic parameters (relative permittivity and conductivity) of all elements in the environment were extracted from ITU [ITU], used to calculate the refection and penetration losses based on the Fresnel formula and served as input to the ray tracing tool to simulate the industrial propagation channel.

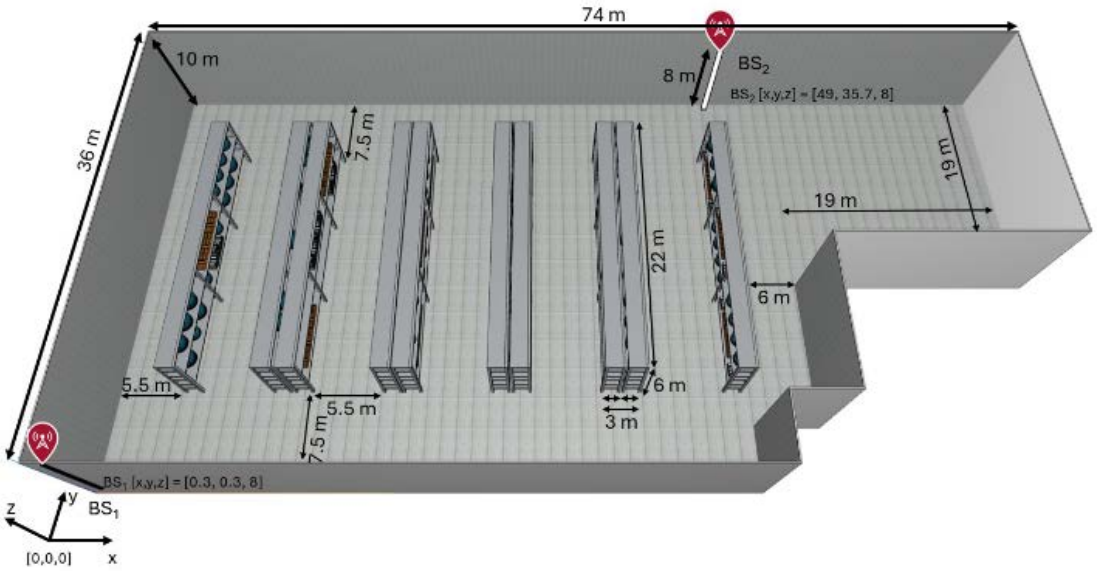

Figure 25: Area under study of 74x36 m in Fabriek Logistiek, Ghent. The industrial scenario contains racks filled with metal, wood, and plastic tanks containing water. Red pins represent the BSs locations.

We modeled here a realistic 5G-NR **Base Station** (BS) operating at 28 GHz in the FR2 band. The BS uses a rectangular array of vertically polarized half-wave dipole antennas with a half-wavelength uniform inter-element spacing ($\lambda \simeq 11$ mm at 28 GHz). We here evaluated different MIMO array sizes (2x2, 4x4, 6x6, 8x8, and 10x10). The BS station height is 8m. The antenna's directivity pattern is presented in Figure 26. The technical parameters of the base station are listed in Table 11.

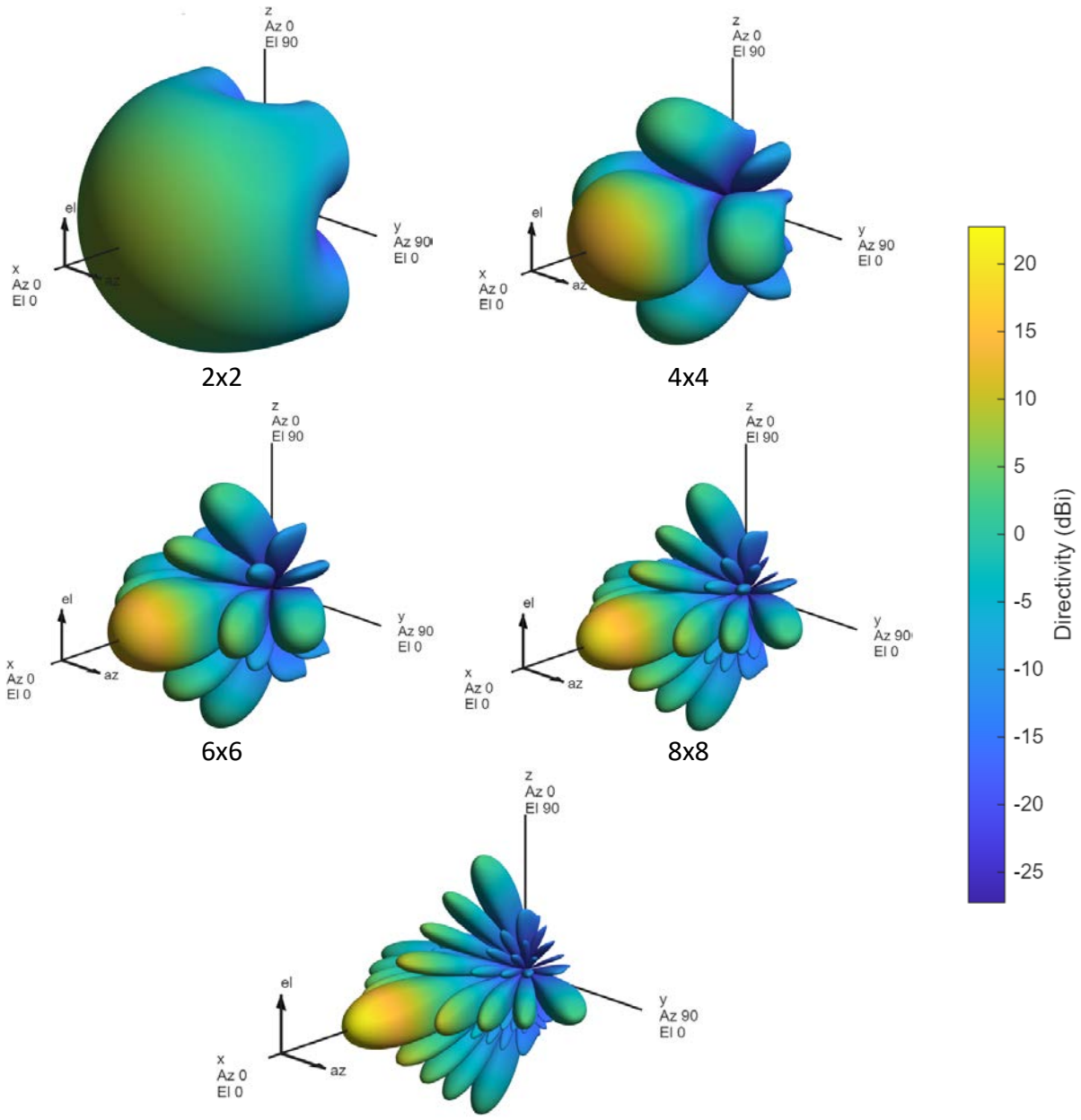

Figure 26. 3D directivity pattern of modelled antenna

Table 11. base station technical parameters for FR2 warehouse Belgium scenario

Location description	
type of location	warehouse – factory
type of installation	private test site
Antenna parameters	
antenna type	directional
antenna gain [dBi]	Max 24.7 dBi, see Figure 26
location of antenna	on wall
antenna height (middle) [m]	8
antenna size	Array size from 5.5 x 5.5 mm (2x2) up to 49.5 x 49.5 mm (10x10)
downtilt [°]	0
envelope of radiation pattern in use	Beamforming with variable radiation pattern
Cell parameters	
type	5G
frequency band	FR2
central frequency [MHz]	28000
MIMO configuration	2×2 up to 10x10
antenna array input power [dBm]	30
duty cycle	1

Multiple-input multiple-output (**MIMO**) with codebook-based beamforming simultaneously generates a subset of a predefined set of beams (the 'codebook') at a time for each antenna element. The signals from all antenna elements are combined into a single signal path (analog beamforming) and then processed at a single receiver or transmitted from a single transmitter, which adjusts the overall beam direction. User equipment (UE) uplink (UL) signaling is processed at the base station (BS) to choose the beam that optimally serves the UE's location. In line-of-sight (LoS) conditions, the beam with the closest direction of departure (DoD) to the true direction of the UE was selected. However, in non-line-of-sight (nLoS) conditions, the largest portion of the RF-EF power might reach the UE through interactions with the propagation environment (e.g., refections or diffractions), and thus the DoD of the beam chosen by codebook-based precoding does not necessarily correlate with the direction of the direct path to the UE. Figure 26 shows the realized antenna pattern at 28 GHz. In this case the azimuth and elevation patterns are equal. The higher the number of elements in the array (up to a certain limit), the greater the gain, resulting in superior signal strength and reliability for the same transmitted power (30 dBm). E.g., a 10x10 MIMO array (24.7 dBi at maximal gain 0° here) offers around 24 times the Signal to Noise Ratio (SNR) compared to a 2x2 MIMO array (10.1 dBi at 0°). Further, a 10x10 MIMO system provides a narrower and main lobe (Half Power Beam Width (HPBW) = 10.2° in the azimuth plane), allowing for better signal directionality and reduced interference compared to a 2x2 MIMO system (HPBW = 59.9° in the azimuth plane). These enhancements make 10x10 MIMO systems more suitable for high-data rates demanding and high-density communication environments. Table 12 summarizes all parameters related to the arrays used in this research.

Beamforming is a technique used in wireless communication to enhance the signal-to-noise ratio (SNR) in a specific direction by adjusting the phase and amplitude of the transmitted signals at the antenna terminals, minimizing interference, and directing the signals toward specific receivers. This produces a reduction in the antenna gain in any other direction but the main direction (see Figure 27b and Figure 27c, and the gain values in Table 12), improving signal quality, extending the signal range, and reducing the amount of received signal power for non-users.

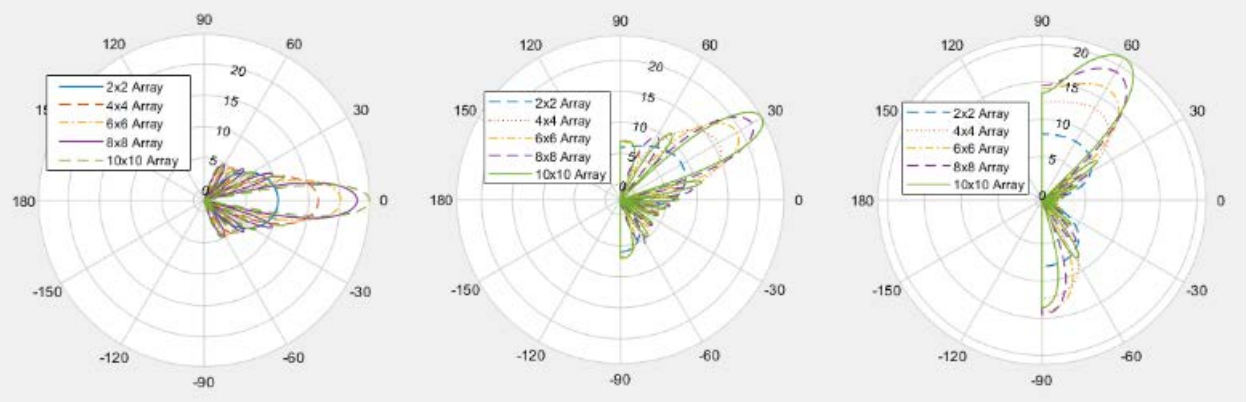

Figure 27. Azimuth and elevation radiation pattern for the different MIMO arrays. a) Without beamforming, pointing at 0°. b) Beamformed to 30°. c) Beamformed to 60°.

Table 12. MIMO array parameters, where gain at 30° (60°) is the antenna gain after beamforming the antenna 30° (60°) away from the 0° direction. HPBW = Half Power Beam Width at 0°.

Array	Number of elements N	Gain at 0° (dBi)	Gain at 30° (dBi)	Gain at 60° (dBi)	HPBW (°)
2x2	4	10.1	9.0	8.2	59.9
4x4	16	16.5	15.8	13.3	26.3
6x6	36	20.7	19.3	16.5	17.2
8x8	64	22.0	22.1	19.1	12.8
10x10	100	24.7	24.0	21.3	10.2

To calculate the electromagnetic properties in the environment, we used MATLAB's 3D Raytracing (RT) tool as described in Section 2. To build the **beamforming table**, we determined the antenna direction yielding the highest received power at the receiver. To that end, we steered the beam of each BS antenna, identify all the rays arriving at the receiver, and chose the Angle of Departure (AoD) for the ray with the lowest PL. To construct the beamforming table, we used the RT algorithm (see previous paragraph) and steered the beam from 0° to 90° in the azimuth plane and from 0° to -90° in the elevation plane for BS1. For BS2, the beam was steered from 0° to 180° in the azimuth plane and from 0° to -90° in the elevation plane. An angular resolution of 3° for

the beamsteering table appeared to be a good tradeoff between calculation time and precision. The resulting beamforming table for this scenario contains the receiver coordinates, the BS that best served the receiver (the one with the lowest PL between the BS and Rx), and the BS's AoD (azimuth and elevation angles for delivering the highest amount of signal at the Rx).

As a **metric** for assessing the exposure values at location Li, we based ourselves on the Downlink (DL) Incident Power Density at Li (S_{Li}) due to the set of N_{BS} base stations (W/m²):

$$S_{Li} = \sum_{x=1}^{N_{BS}} \frac{E_{Li,BSx}^2}{377}.$$

$E_{Li,BSx}$ (V/m) is the electric field generated by base station x (BSx) at location L_i, and is calculated as the root of the squared sum of the E of the different rays arriving at Li: $E_{Li,BSx} = \sqrt{\sum_{j=1}^{J} E_{Li,BSx,j}^2}$, with J the number of considered rays. $E_{Li,BSx,j}$ is derived from the path loss along ray j between BSx and Li ($PL_{BSx,Li,j}$) (dB):

$$E_{Li,BSx,j} = 10^{\frac{EIRP_{BSx,j}+10log_{10}DC_{TDD}^{DL}-43.15+20log_{10}f_{BSx}-PL_{BSx,Li,j}}{20}}$$

where $EIRP_{BSx,j}$ (dBm) is the EIRP of BSx assuming the gain along ray j. This gain will depend on the steering direction of the beam. f_{BSx} is BSx's frequency (MHz), DC_{TDD}^{DL} is the Time-Division Duplex (TDD) duty cycle in the downlink. As we characterized the user's worst-case RF exposure, we considered TDD equal to 1. ICNIRP has set a six-minute averaging time for RF-EF and established occupational exposure limits at 28 GHz of 152 W/m² and a limit for the general public of 30.5 W/m² [ICNIRP].

3.1.7.2 Simulation scenarios

In all **scenarios**, we considered the presence of two BSs, which suffices to provide at least -75 dBm everywhere, corresponding to a maximum throughput of 385 Mbps for a 5G network deployment [Santana]. This data rate matches with the general requirements for low-latency Augmented Reality applications, which is considered as a future high-throughput application in an industrial context. The input power to the antenna was 30 dBm. We further assumed that one BS was active while serving the user, and the other BS remained in standby. When the received signal from the BS in standby became higher than that from the currently active BS (according to the beamforming table), they switched the active and stand-by conditions and the user was served by the other BS. These configurations formed the basis for the following three exposure analyses.

1. User vs non-user exposure

To calculate the incident power density S at each possible location, we assumed the receiver (Rx) was a single-terminal device equipped with a vertically-oriented, vertically-polarized half-wave dipole antenna. The potential Rx locations were arranged on a regular rectilinear grid with 3-

meter spacing in both the x and y directions and are positioned at a height of 1.7 meters above the ground plane (along the z-axis). This setup formed an evaluation grid of 218 locations uniformly spaced 3 meters apart, excluding those obstructed by racks. This grid arrangement allowed obtaining a statistical distribution of exposure values across different potential user (operator) locations. Beamforming ensured optimal signal delivery to user locations, and the beamforming table stored the AoD to optimally serve each location. User exposure was defined as the incident power density at the user's location when the antennas' beam was optimally steered toward that location. In contrast, non-user exposure was defined as the incident power density at any of the other 217 locations at which the user was not located. In general, and for statistical representativeness, we considered the average non-user exposure over all 217 non-user locations.

2. Spatial duty cycle

The spatial duty cycle (DC^{SPA}) concept was used for comparing exposure levels for users and non-users. It provides a specific metric to evaluate exposure levels in environments with beam-steering antennas or phased array systems, such as those used in millimeter-wave (mmWave) and 5G networks. DC^{SPA} quantifies the relative RF exposure at a specific location L when the antenna beam is directed elsewhere (non-user case) versus when it is fully focused on that location (connected user case). It provides a percentage-based measure of how beamforming affects exposure levels at various locations. This ratio is dependent on the considered location Li in the area with i = 1... 218. Hence, for the considered area, 218 spatial duty cycle values were obtained. Concretely, spatial duty cycle at L_i (DC_{Li}^{SPA}) was defined as:

$$DC_{Li}^{SPA} = 100\frac{S_{Li}^{non-user}}{S_{Li}^{user}}(\%)$$

where $S_{Li}^{non-user}$ (W/m^2) represents the power density at location Li when the antenna is steered towards the other possible locations averaged over the (here 217) other locations, with an index different from i. S_{Li}^{user} (W/m^2) is the maximum power density at Li, i.e., when the beam is optimally directed there. This gives a quantification of the exposure at a given location (Li) when the antenna beam was pointed towards the user (i.e., user is connected) versus when the antenna beam was pointed to an (average) other location (i.e., user is not connected).

3. Spatiotemporal duty cycle

Spatio-temporal duty cycle ($DC^{SPA\text{-}TEMP}$) is a function of the actual connection time and of the spatial duty cycle at the considered location, which was determined by the exposure when being considered a connected user (i.e., actively attracting the beam) and the exposure when considered to be a non-user (i.e., not connected, with the beam pointing elsewhere). This metric is particularly useful in analyzing intermittent activity over time and is essential for applications in 5G networks, where service scheduling time is often a fraction of the total RF exposure averaging time. Similar to literature, we introduced *Ts* to represent the duration of one

connection (often referred to as "scheduling time"). In this research, we assumed the base station (BS) was operating continuously during the 6-minute period *T* (i.e., T=360s, 100% of the time). For each N (number of antenna elements), we examined connection durations *Ts* of 60s, 10s, 1s, and 0s. Then, the spatiotemporal duty cycle at location Li was defined as:

$$DC_{Li}^{SPA-TEMP} = 100\frac{S_{(Li,Ts)}^{average}}{S_{Li}^{user}}(\%)$$

where $S_{(Li,Ts)}^{average}$ is the average exposure of the person at Li when being connected (i.e., beam optimally steered towards Li) for a duration of *Ts* within a time window *T*. It was calculated as the weighted average of the incident power density at Li when the user is connected (i.e., S_{Li}^{user}) and the incident power density when the user is not connected (i.e., $S_{Li}^{non-user}$), each weighted by the fraction of the time the situation holds.

$$S_{(Li,Ts)}^{average} = \frac{T_s}{T}S_{Li}^{user} + (1-\frac{T_s}{T})S_{Li}^{non-user}$$

Ts/T is often defined as the temporal duty cycle (DC^{TEMP} = *Ts/T*). Combining the previous two equations lead to the following expression:

$$DC_{Li}^{SPA-TEMP} = DC^{TEMP} + DC_{Li}^{SPA} - DC^{TEMP}.DC_{Li}^{SPA}$$

The spatiotemporal duty cycle metric complements DC^{SPA} by incorporating temporal factors into the assessment of spatial RF exposure. This integration captures both location-based and time-based characteristics in environments with dynamic beam-steering systems or fluctuating user demand. We simulated all 218 locations within an industrial environment calculating for each location the spatiotemporal duty cycle for different connection durations *Ts*. To characterize duty cycles over the entire considered area, we used the 95th percentile values of the (218) obtained duty cycles.

3.2 Results

This section describes the results of the different simulation scenarios presented in Section 3.1. After discussing the scenarios individually, we provide a comparison between scenarios.

3.2.1 FR1: 3.6 GHz – indoor smart Industry 4.0

This section discusses the results of the indoor smart Industry 4.0 scenario, for the warehouse and the production hall environment respectively.

3.2.1.1 Warehouse Germany

The exposure due to 4 pRRHs inside the warehouse was calculated with NARDA for the whole area of the warehouse. With the resolution of 0.1 m in NARDA, the results consist of 208 328 calculation points, as shown in Figure 28.

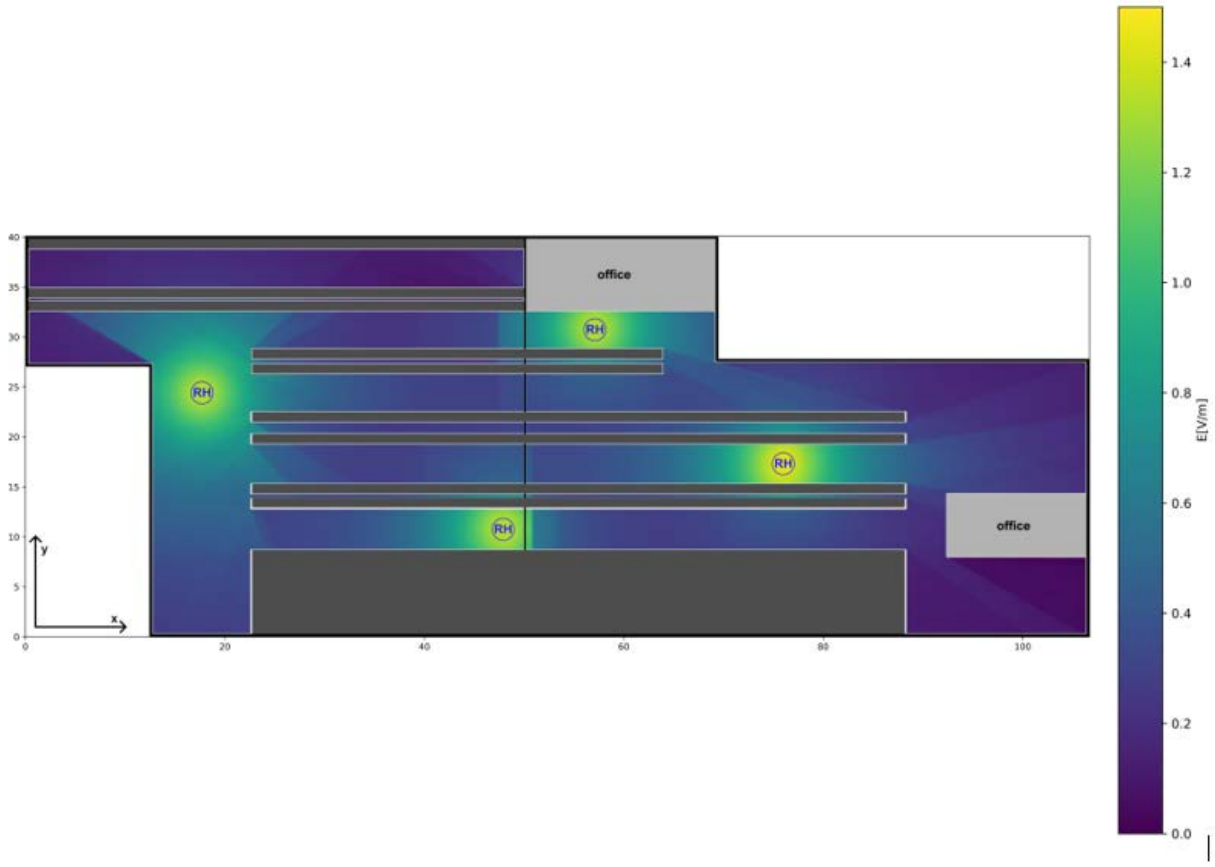

Figure 28. Electric field inside warehouse Germany for NARDA in a horizontal plane at the height of 1.5 m.

For all calculated 208 328 points the maximum value is 1.45 V/m, the 95th percentile is 1.06 V/m, mean value 0.50 V/m, median value 0.34 V/m and standard deviation 0.60 V/m.

3.2.1.2 Production hall

The exposure due to 6 pRRHs inside the production hall was calculated with NARDA for the whole area of the production hall. The resolution of the calculation is 0.1 m, meaning that the results consist of 275 678 calculation points, as shown in Figure 29.

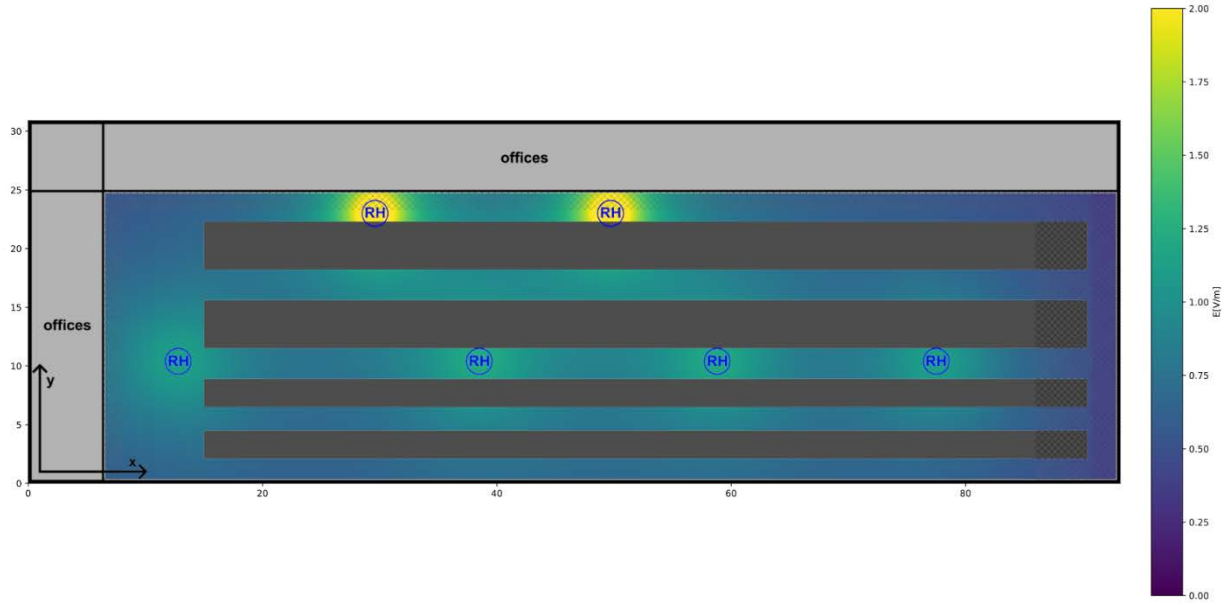

Figure 29: Electric field inside the production hall. There are 6 pRRHs located inside the production hall, 4 of them mounted on the ceiling and 2 of them on the balcony.

For all calculated 275.678 points the maximum value is 2.72 V/m, the 95th percentile is 1.14 V/m, mean value 0.79 V/m, median value 0.74 V/m and standard deviation 0.77 V/m.

3.2.2 FR1: 3.5 GHz – Port of Koper, outdoor macro cell

The exposure due to beamforming 5G FR1 base station was calculated with NARDA on a large area on a top parking lot of the car garage. The resolution of the calculation is 0.1 m, meaning that the results consist of 1 002 001 calculation points. Numerical modelling was performed for the envelope of traffic channels which represents the worst-case exposure situation, as shown in Figure 30.

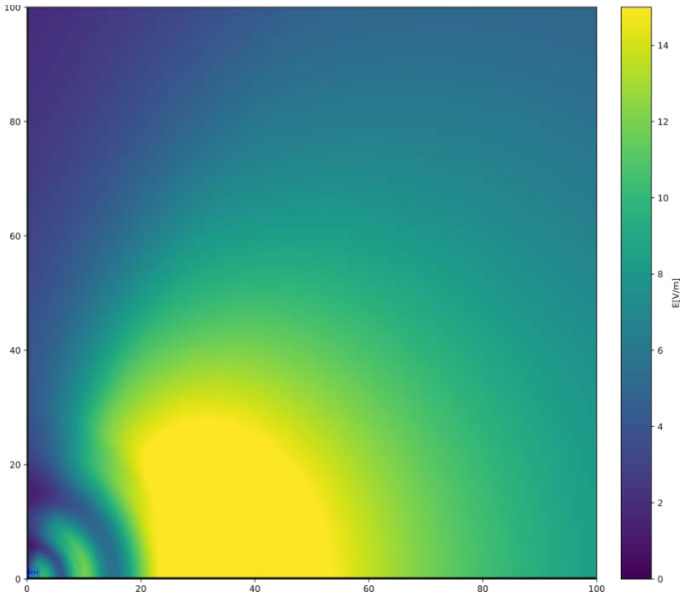

Figure 30: Electric field due to the operation of a FR1 base station with the output power of 100 W in a horizontal plane at the height of 1.5 m.

For all calculated 1 002 001 points the maximum value is 18.49 V/m, the 95th percentile is 15.88 V/m, mean value 9.79 V/m, median value 8.92 V/m and standard deviation 8.39 V/m.

3.2.3 FR1: 3.5 GHz – office, pico cell

The exposure inside an office with a wall mounted 5G FR1 base station with 20 W output power was calculated for the whole area of the office with NARDA. The resolution of the calculation is 0.1 m, meaning that the results consist of 39 501 calculation points, as shown in Figure 31.

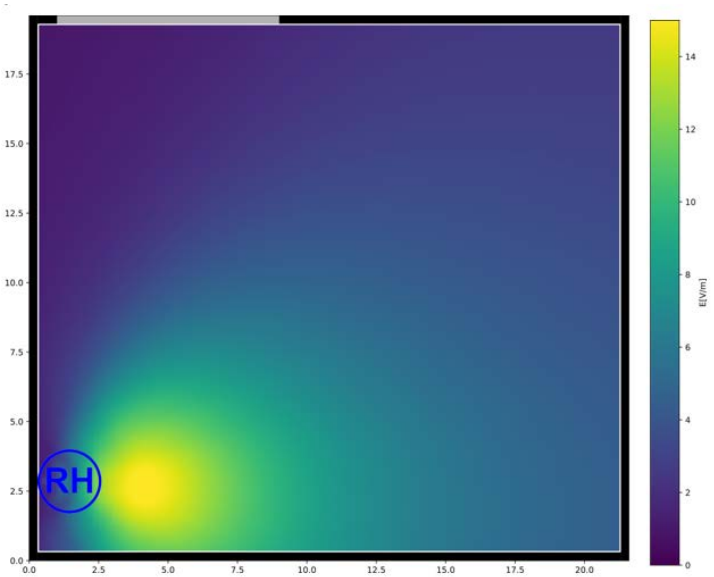

Figure 31. Electric field inside small office for INIS in a horizontal plane at the height of 1.5 m.

For all calculated 39 501 points the maximum value is 15.26 V/m, the 95th percentile is 11.31 V/m, mean value 5.54 V/m, median value 4.01 V/m and standard deviation 6.38 V/m.

3.2.4 FR1: 3.5 GHz – Warehouse Belgium

We simulated the spatial distribution of the electric-field values in the industrial test factory as described in Section 3.1.4. Figure 32 shows the spatial distribution of these E-field values (V/m) for the separate 4G (or 5G) network (left), and for the collocated 4G/5G network (right). The median electric-field values for the 4G and the 5G networks separately equal 2.23 V/m, with a 90th percentile value of 3.56 V/m. For the collocated 4G/5G network, median exposure values amount to 3.15 V/m, with a 90th percentile value of 5.13 V/m.

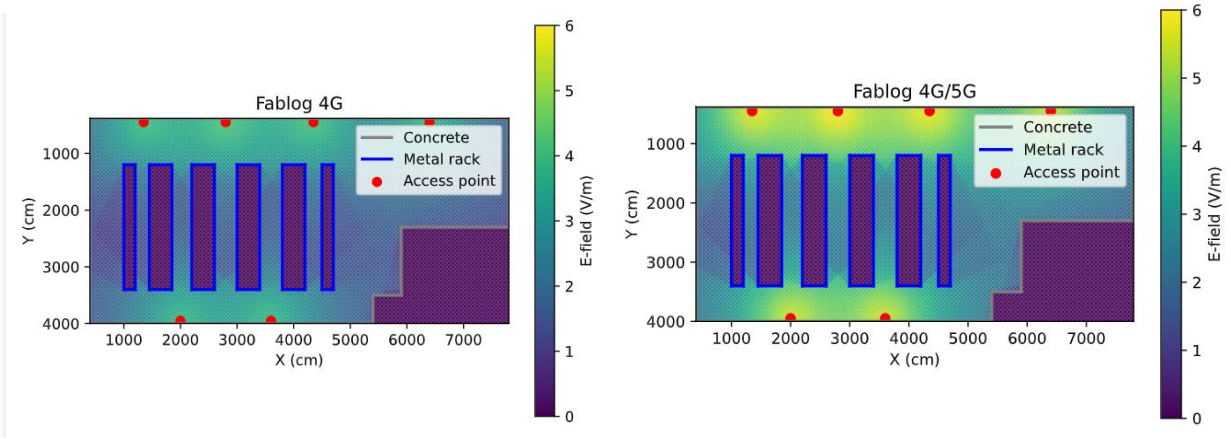

Figure 32: Spatial distribution of E-field values (V/m) in the industrial environment, for the separate 4G (or 5G) network (left), and for the collocated 4G/5G network (right).

3.2.5 WiFi 6: 5.5 GHz – Lab scenario, beamforming

In this section the simulation results on the 3 scenarios that were described in Section 3.1.5.4 are presented. We discuss the effect that WiFi 6 Access Points with beamforming capabilities have on EMF exposure on users and non-users (bystanders).

3.2.5.1 Exposure on workstation positions

The results of the simulations for the first exposure scenario are presented in Table 13, which lists the calculated electric field values at each of the five workstation positions for both the static and beam-steering transmitter configurations, along with their differences expressed in dB. Figure 33 illustrates how the electric field at each position varies depending on the direction of the high-gain beam, i.e., the position of the active user.

Table 13. E-field values at positions A to E with and without beam steering for all active user cases

Position	Static	Beam steering									
	E-field (V/m)	User pos: A		User pos: B		User pos: C		User Pos: D		User Pos: E	
		E-field (V/m)	Diff (dB)	E-field (V/m)	Diff (dB)	E-field (V/m)	Diff (dB)	E-field (V/m)	Diff (dB)	E-field (V/m)	Diff (dB)
A	0.56	**0.93**	**4.43**	0.89	4.03	0.78	2.94	1.06	5.58	1.00	5.03
B	0.27	0.40	3.48	**0.72**	**8.69**	0.78	9.40	0.44	4.48	0.22	-1.74
C	0.71	0.48	-3.35	1.44	6.13	**1.45**	**6.18**	0.99	2.86	0.41	-4.78
D	0.45	0.71	3.92	0.78	4.81	0.76	4.54	**0.91**	**6.09**	0.86	5.61
E	1.38	1.37	-0.11	0.32	-12.71	0.24	-15.08	0.97	-3.12	**1.90**	**2.75**

At positions A and D, the electric field is consistently higher in all beam-steering cases compared to the static radiation pattern, regardless of which position the antenna is directed toward. In contrast, at position E, the electric field is always lower in the beam-steering configuration, except when the beam is directed toward position E itself, where an increase is observed. At position C, an increase in electric field is observed not only when the beam is directed toward C, but also when it is steered toward positions B and D. At position B, the electric field generally increases with beamforming, with the only slight decrease occurring when the antenna is steered toward position E. These results are visually presented in Figure 33.

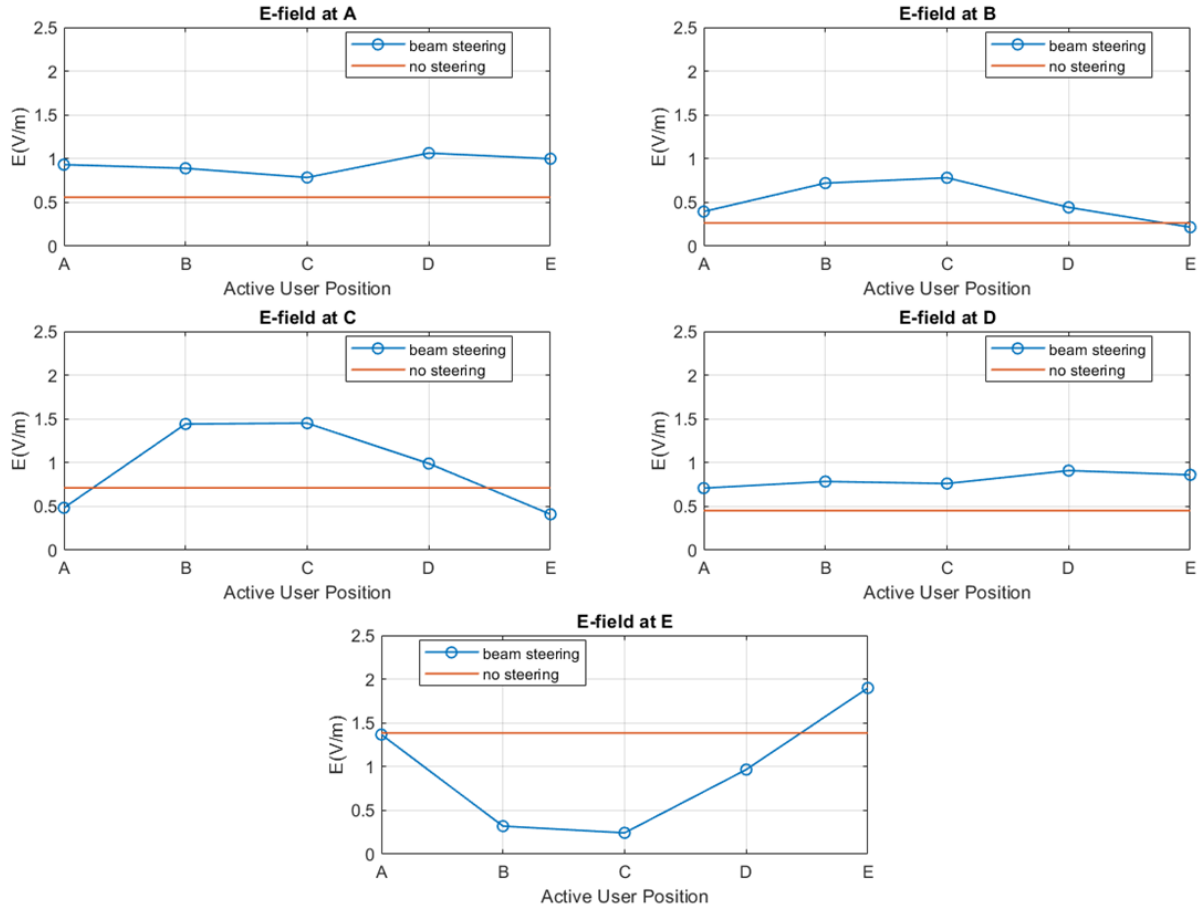

Figure 33. Calculated E-field at each position as a function of active user position

Figure 34 below illustrates the effect of beam steering on users and bystanders, presented separately. For bystanders, the RMS electric field value at each position was calculated based on the electric field values obtained when the antenna was steered toward all active user positions except the respective bystander's location.

As expected, a substantial increase in exposure is observed for active users, ranging from 2.7 dB at position E to nearly 9 dB at position B. In the case of bystanders, an increase in electric field was observed at 4 out of the 5 positions, with the largest occurring at position B where it exceeded 5 dB. The only decrease in bystander exposure was observed at position E, where the electric field dropped by approximately 4 dB when beam steering was applied.

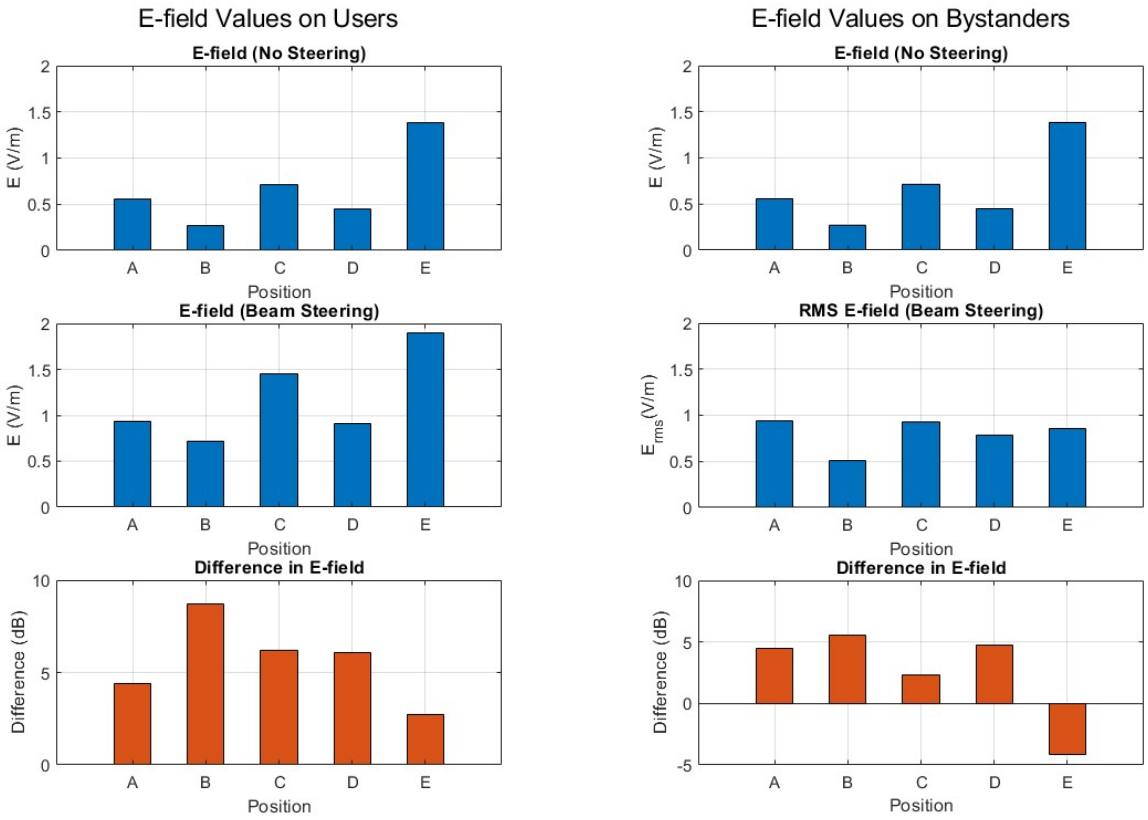

(a) (b)

Figure 34. Difference between static and beamforming transmitter on a) users and b) bystanders

3.2.5.2 Exposure on moving active user and workstations

Figure 35 presents the simulation results of the second scenario, which involves a moving user and four bystanders located at workstation positions A, C, D, and E. As in the previous scenario, the electric field was calculated for two cases: one with the transmitting antenna using a static radiation pattern, and another where a high-gain beam is steered toward the moving user.

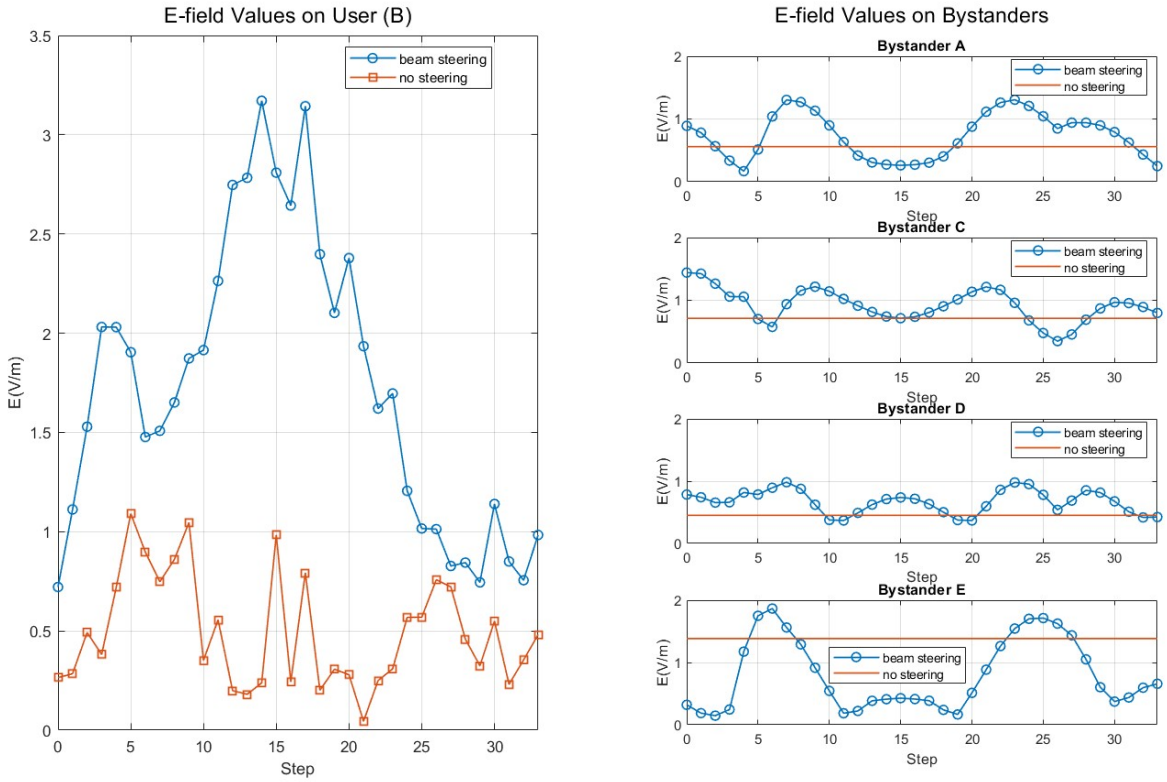

(a) (b)

Figure 35. User (a) and bystanders (b) E-field at each step of the user's route

For the user, there is a significant increase in exposure when comparing the static and beam-steering transmitting antennas, as also illustrated by the cumulative distribution function shown in Figure 36. The median value increased by 12 dB, while the 95th percentile value increased by 9.5 dB.

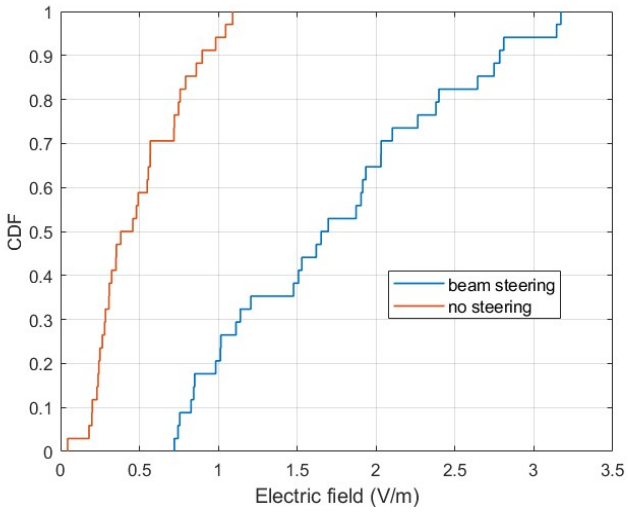

Figure 36. CDF of the moving user

For bystanders, exposure increases when the antenna is steered toward the moving user in 3 out of 4 cases. At bystander position A, 62% of the electric field values exceed the corresponding value obtained with the static radiation pattern. This proportion is even higher for bystanders C and D, with 77% and 81% of the values, respectively, being greater than those in the static case. Only at position E is the total exposure reduced: just 22% of the electric field values exceed the level that would occur with a static radiation pattern.

Table 14 presents the RMS electric field at each bystander position when the antenna is steered toward the moving user, compared to the static radiation pattern case.

Table 14. E-field values at bystanders positions

Bystander Position	Static E-field (V/m)	Beam steering RMS E-field (V/m)	Difference (dB)
A	0.56	0.81	3.26
C	0.71	0.96	2.55
D	0.45	0.70	3.76
E	1.38	0.98	-3.02

When beam steering is applied, the differences in bystander exposure tend to smooth out, as the RMS values of the electric field across the bystander positions appear to converge. This indicates that the dynamic nature of the radiation pattern distributes energy more evenly over time as the user changes position compared to the static case.

The impact of beamforming on bystander exposure is largely influenced by the initial exposure levels observed with the static radiation pattern. Specifically, similar to what was observed in Scenario 1, we see an increase in exposure at positions A, C, and D, the locations where the electric field was relatively low in the static case. Conversely, at position E, where the static field strength was already relatively high, beamforming results in a decrease in exposure. This suggests that beamforming can both amplify or reduce exposure at a given location.

3.2.5.3 Generalized exposure assessment

In the final scenario, the electric field was calculated at randomly distributed locations covering the entire laboratory area. Figure 37 presents a heat map of the electric field distribution across these locations, providing a spatial overview of exposure levels throughout the environment. In this figure, the user's position is indicated by an arrow originating from the access point, representing the direction in which the high-gain beam is steered during each simulation instance.

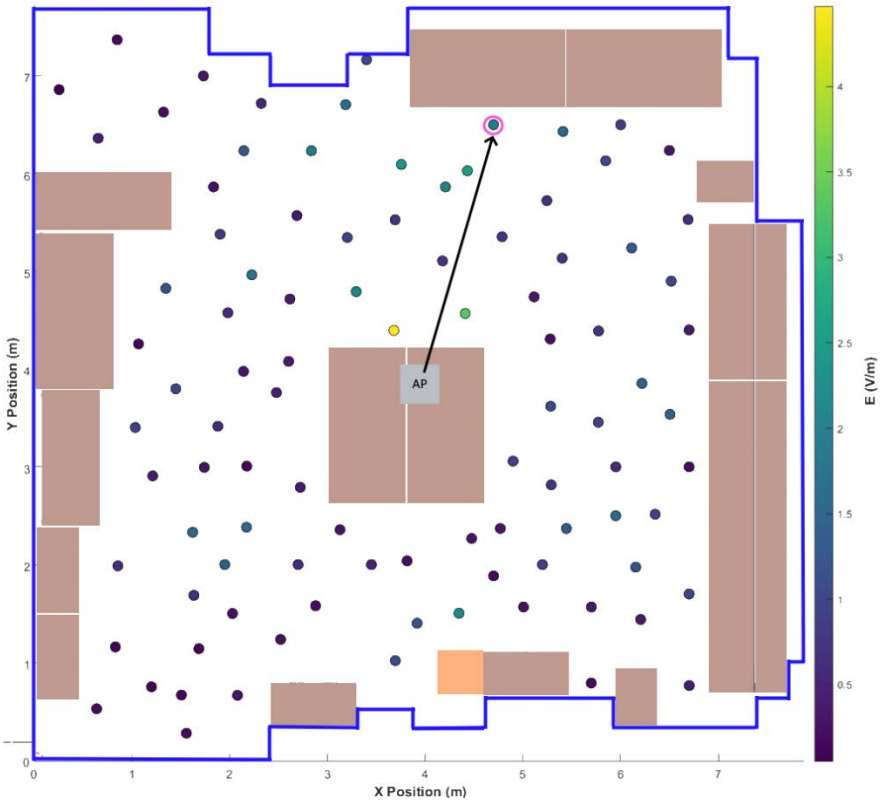

Figure 37. E-field values with transmitter steered towards specific user location

Figure 38 presents the cumulative distribution function for users' and bystanders' exposure with a beam steering transmitter antenna as well as the exposure on the same random locations with a non-steering antenna.

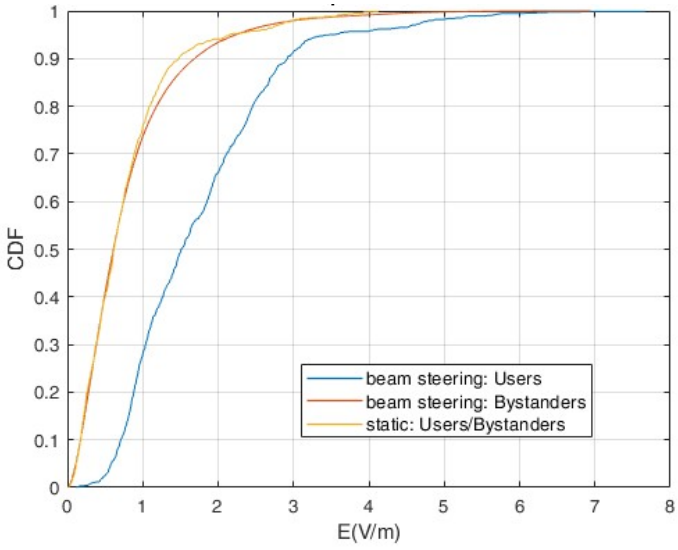

Figure 38. CDF of the user and bystanders with beam-steering antenna and static radiation pattern antenna

For the users/bystanders, when the antenna had a static radiation pattern, the 50th and 95th percentiles of the calculated electric field were 0.62 and 2.19 V/m respectively. In the beam-steering antenna case, the corresponding values were 0.61 and 2.24 V/m for the bystanders, and 1.51 and 3.52 V/m for the users.

From Figure 38, we observe that the distributions for the bystanders are almost identical in the beam-steering and static (non-steering) cases. The differences between the 50th and 95th percentile values are minimal (-0.18 dB and 0.2 dB, respectively). Therefore, we can conclude that in our case, the bystanders' exposure is generally unaffected by the use of a beam-steering antenna.

As expected, the exposure for the active user increased significantly, with the 50th percentile rising by 7.7 dB and the 95th percentile by 4.1 dB.

When comparing user and bystander exposure in the beam-steering case, the user's exposure exceeds that of bystanders by 7.9 dB at the 50th percentile and by 3.9 dB at the 95th percentile. While this increase is notable, it is lower than what has been reported in the literature and in the 'FR2: 28 GHz –warehouse Belgium, beamforming' scenario referenced in this document. This discrepancy is most likely due to differences in the transmitting antenna's radiation pattern. In our case, the antenna does not produce a single dominant, highly directional beam but instead radiates several lobes in various directions, resulting in a pattern that is closer to omnidirectional. As a consequence, unintended high-gain lobes intermittently point toward bystander positions, increasing their exposure even though they are not the intended target.

3.2.5.4 Conclusion

For this exposure scenario, we tried to assess the maximum exposure of employees inside a laboratory where a WiFi 6 network is operating. We considered 3 different scenarios and we focused on the differences between beam-steering and static transmitting antennas on the active users of the network and the bystanders. We found that beamforming significantly increases the exposure of users as was expected. For bystanders, the impact of beamforming was less straightforward. In our first two scenarios where the bystanders had specific locations inside the laboratory, we observed an increase in most cases but not all. The variation mainly depended on the circumstantial relative position with reference to the transmitter and therefore their exposure levels with a static radiation pattern. In the third generalized scenario, which considered a large number of positions throughout the laboratory, the application of beamforming did not affect bystander exposure.

As previously stated, these scenarios were designed to assess the maximum potential exposure. In real-world conditions, however, we expect the average exposure to be lower when beamforming is employed. This is because the more focused and powerful signal received by the active users improves the signal-to-noise ratio (SNR) and reduces interference, enabling higher data rates. As a result, the duty cycle can be reduced, or, if the access point has power

management enabled, the transmitted power may be dynamically lowered. These factors contribute to an overall reduction in average EMF exposure despite the localized increases observed in worst-case beamforming scenarios.

3.2.6 FR2: 26 GHz – Lab scenario, beamforming

The exposure inside the anechoic chamber due to beamforming 5G FR2 base station was calculated for the whole area of the chamber using NARDA. The resolution of the calculation is 0.1 m, meaning that the results consist of 14 641 calculation points. Numerical modelling was performed for the envelope of traffic channels which represents the worst-case exposure situation, as shown in Figure 39.

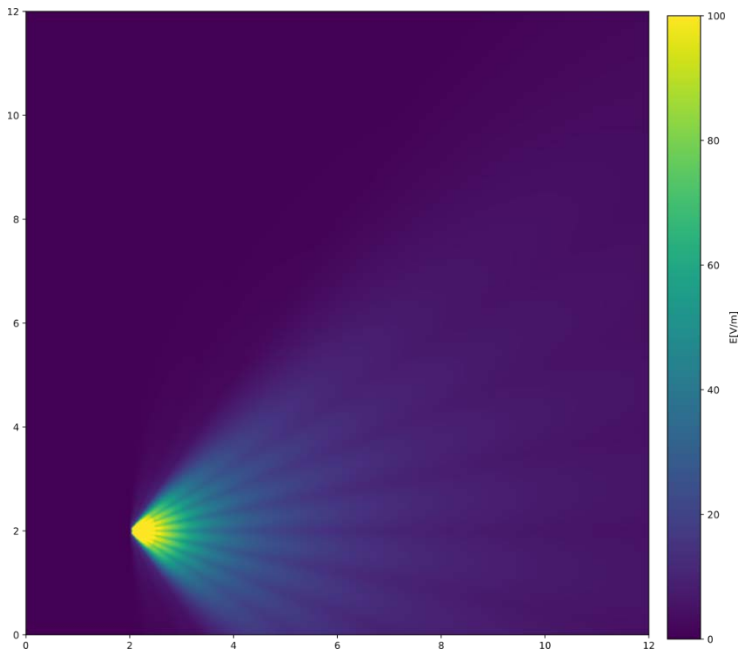

Figure 39. Electric field due to the operation of a FR2 base station with the output power of 1 W in a horizontal plane at the height of 1.5 m, which is also the height of the centre of the antenna.

For all calculated 14 641 points the maximum value is 205.31 V/m, the 95th percentile is 19.68 V/m, mean value 10.99 V/m, median value 3.27 V/m and standard deviation 27.33 V/m.

3.2.7 FR2: 28 GHz –Warehouse Belgium, beamforming

This section extensively discusses the simulation results in the industrial test factory, as described in Section 3.1.7. Three main topics are analyzed: the difference of user vs. non-user exposure, the spatial duty cycle in the area, and the spatiotemporal duty cycle.

3.2.7.1 User vs. non-user exposure

Figure 40a and 40b show the incident power density heat map when BS2 is serving one (NLoS) location (highlighted with magenta circles), for two different MIMO arrays (2x2 and 10x10). In both cases, the BS's antenna used the same AoD confirming that the beamforming table was built with the optimal AoD for reaching the receivers. In this case the user's incident power density is 20.3 times higher when a 10x10 array is used (S = 33.7 mW/m^2) than when a 2x2 array is used (S = 1.66 mW/m^2). Figure 40c shows the cumulative distribution function (CDF) of the incident power density S of all locations in the area, including the user location and for both arrays. It confirms that using a 10x10 array the user is more exposed (higher 95th percentile for 10x10 than 2x2 array), but the non-users' position are less exposed (lower 50th percentile for 10x10 than 2x2 array).

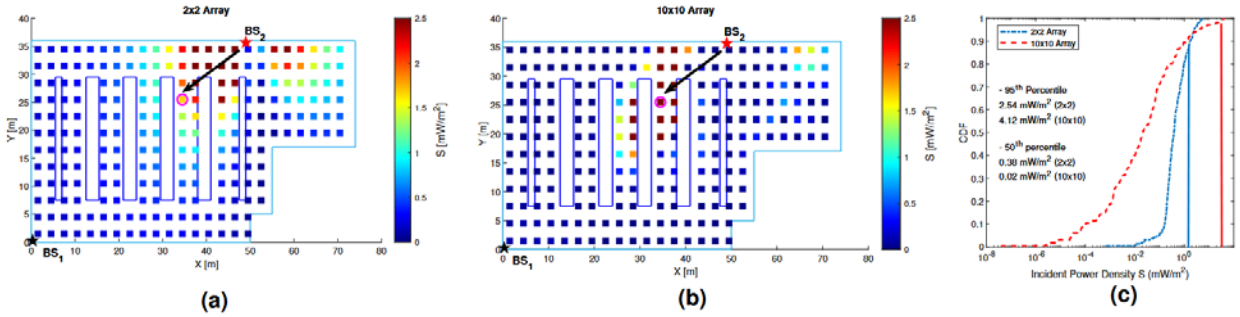

Figure 40. Power density (S) values when array is serving the user (indicating with magenta circle) for (a) a 2x2 MIMO array and (b) a 10x10 MIMO array. c) Cumulative Distribution Function (CDF) of the incident power density S in the area for both arrays. Black arrows show the BS's Angle of Departure (AoD).

To extend the analysis, we calculated the exposure level for user and non-users' locations over the entire area. In this scenario, this corresponds to 218 possible user locations, each having non 217 non-user locations. Figure 41 shows the cumulative distribution function for users' and non-users' exposure for the different arrays showing the distribution of user and non-user exposure when both the user and the non-user were randomly located in the area.

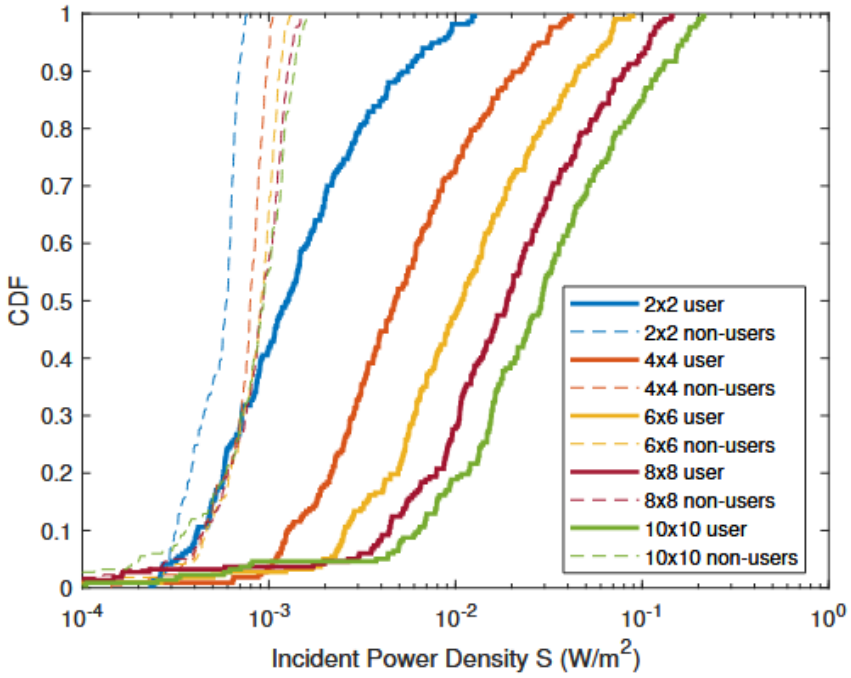

Figure 41. CDF of the user and non-user exposure for randomly located users and non-users in the area.

Table 15 summarizes the 95th and 50th percentiles of the incident power density for user and non-user exposure. The table shows that the exposure difference between user and non-user for the 95th percentile ranges from 91% to 99% and from 53% to 97% for the 50th percentile depending on the array size. It also shows that as the array size increases from a 2x2 configuration to a 10x10 configuration, there is a substantial increase in both the 95th (around 21 times from 2x2 to 10x10) and 50th (around 23 times from 2x2 to 10x10) percentile values of incident power density for users. In comparison, the increase in incident power density for non-users is lower than that for users. While the 95th percentile values for non-users increase slightly (around two times from 2x2 to 10x10), the 50th percentile values increase around 1.5 times as the array size increases. This indicates that non-users receive relatively similar exposure regardless of the array size, likely reflecting incidental exposure rather than direct targeting by the array. Then, we can partially conclude that larger arrays, likely due to more focused beamforming capabilities, lead to higher exposure for users and higher difference in the exposure level between user and non-users. Another factor that influences in the user and non-users' exposure level is when the racks inside the scenario are filled with different materials. For user's locations, when the racks are filled with different materials the exposure level increase between 2% and 7% for the different array sizes. In this case the racks contents add reflective contribution to user's locations. In the case of non-user's locations, when the racks are filled with different materials the exposure level decrease between 0.5% and 3% for the different array sizes. This is because the racks contents block the amount of signal arriving to the non-users' locations. In [Shikantsov2023], the authors found the exposure of non-users compared to active users using distributed massive MIMO was one to two orders of magnitude lower. Our results align with [Shikantsov2023], where the

exposure of non-users compared to active users ranges from 1 (for 2x2 array) to 2.1 (for 10x10 array) orders of magnitude lower.

Table 15. 95th and 50th percentiles of the incident power density S (mW/m^2) values for users and non-users in the area for empty racks, and reduction percentages for non-users vs users.

	User		Non-users	
Array size	**95th percentile**	**50th percentile**	**95th percentile**	**50th percentile**
2x2 array	7.94	1.26	0.72 (-91%)	0.59 (-53%)
4x4 array	29.97	4.75	1.01 (-97%)	0.80 (-83%)
6x6 array	65.48	10.77	1.20 (-98%)	0.91 (-91%)
8x8 array	109.73	18.87	1.35 (-99%)	0.93 (-95%)
10x10 array	163.82	28.79	1.46 (-99%)	0.93 (-97%)

3.2.7.2 Spatial duty cycle

Figure 42a and 42b display the spatial duty cycle (DC^{SPA}) for the five arrays under test for empty and for filled racks). The results show that larger arrays significantly contribute to exposure reduction across the area, with 95th percentile of the DC^{SPA} values decreasing from 45% to 10.5% in the empty-rack scenario and from 45% to 9.1% in the filled-rack scenario when moving from a 2x2 to a 10x10 array. This reduction corresponds to a lower proportion of high-exposure locations, particularly benefiting non-users by lowering their exposure levels in comparison to smaller arrays.

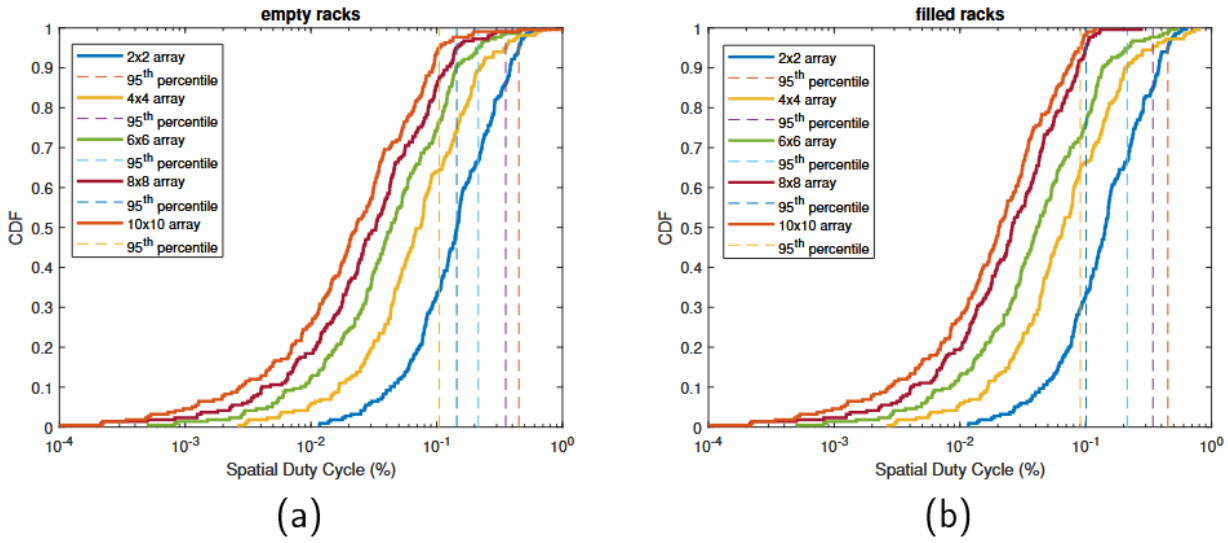

Figure 42. CDF of spatial duty cycle (%) for all the possible locations in the area. a) empty racks. b) filled racks

Table 16 summarizes the 95th and 50th percentiles of the spatial duty cycle for empty and filled racks. It shows that median values are, on average (over all arrays), only 0.5% higher for empty racks compared to filled racks. In the case of the 95th percentile values, they are, on average (over all arrays), 1.4% higher for empty racks. This is because rack contents add reflective

contributions when the location Li is considered as the user and reduce (by blocking the signal) the exposure for the non-user case (when the BS is pointing elsewhere).

Table 16. 95th and 50th percentiles of the DCSP A for empty and filled racks

	Empty racks					Filled racks				
DC^{SPA}	**2x2**	**4x4**	**6x6**	**8x8**	**10x10**	**2x2**	**4x4**	**6x6**	**8x8**	**10x10**
50^{th} percentile	14.5	7.4	4.4	3.3	2.3	14.2	6.6	4.1	2.6	2.0
95^{th} percentile	45.0	35.4	21.4	14.4	10.5	45.0	34.2	21.4	10.1	9.1

Figure 43a and 43b show a spatial map of the DC^{SPA} in the environment (empty racks) for a 2x2 and a 10x10 array respectively. We observe that DC^{SPA} is higher for locations further from the BSs. This can be explained that while non-user exposure is relatively homogeneously distributed over the entire area, user exposure decreases with increasing distance from the BSs leading to a higher DC^{SPA}. Finally, both figures exhibit the same pattern but show lower DC^{SPA} values for larger array sizes.

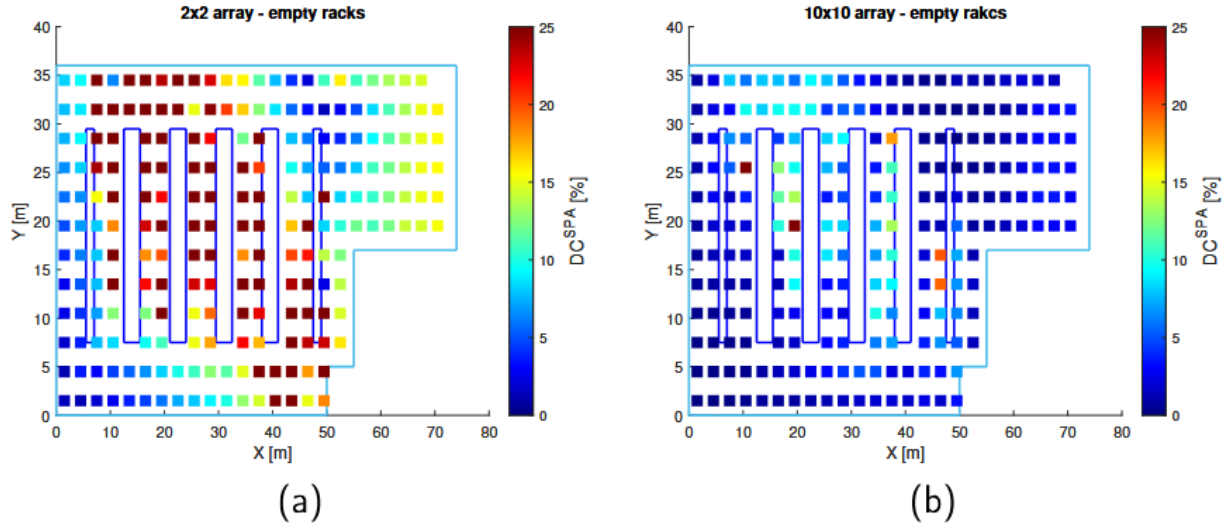

Figure 43. Spatial duty cycle (%). a) DC_{SPA} for a 2x2 array. b) DC_{SPA} for a 10x10 array.

3.2.7.3 Spatiotemporal duty cycle

Table 17 shows the 95th percentiles of the spatiotemporal duty cycle for different array sizes, for racks that are either empty or filled, and for connection durations Ts of 60s, 10s, 1s, and 0s which represent 16.6%, 2.8%, 0.3%, and 0% of the 6-minutes period, respectively. As the antenna array size increases, the 95th percentile values of the duty cycle consistently decrease for both empty and filled racks across all exposure times. It confirms that increasing the array size is an effective strategy for lowering (from 54% to 11% for empty racks and from 54% to 9% for filled racks) the spatiotemporal duty cycle in the area. The more elements in the array, the more concentrated the energy toward the user, thereby lowering the duty cycle [Shikantsov2023]. The same

conclusions as for the spatial duty cycle can be made regarding array size resemblance of empty racks vs. filled racks values, and spatial trends of the spatiotemporal duty cycle on the map.

Table 17. 95th percentile of the spatiotemporal duty cycle ($DC_{p95}^{SPA-TEMP}$) in % for Ts ∈ {60s, 10s, 1s, 0s} for empty and filled racks.

	Empty racks					Filled racks				
$DC_{p95}^{SPA-TEMP}$	**2x2**	**4x4**	**6x6**	**8x8**	**10x10**	**2x2**	**4x4**	**6x6**	**8x8**	**10x10**
Ts = 60 s	54.2	46.2	34.5	28.7	25.4	54.2	45.2	34.5	25.1	24.2
Ts = 10 s	46.6	37.2	23.6	16.8	13.0	46.6	36.0	23.6	12.6	11.6
Ts = 1 s	45.2	35.6	21.7	14.7	10.7	45.2	34.4	21.6	10.3	9.3
Ts = 0 s	45.0	35.4	21.4	14.4	10.5	45.0	34.2	21.4	10.1	9.1

To generalize towards the influence of the temporal duty cycle on spatiotemporal duty cycle values, Figure 44 shows the variation of the 95th percentile of the spatiotemporal duty cycle ($DC^{SPA-TEMP}$) as a function of the temporal duty cycle (DC^{TEMP}) for the different array sizes. When the connection time is equal to 360s (Ts = 360s), DC^{TEMP} is 100%, and $DC^{SPA-TEMP}$ is also 100% (i.e., 1). This means that the base station is only serving the location Li during the 6 minutes and that location is exposed the maximally 100% of the time. When Ts = 0s, the spatiotemporal duty cycle ($DC^{SPA-TEMP}$) equals the spatial duty cycle (DC^{SPA}).

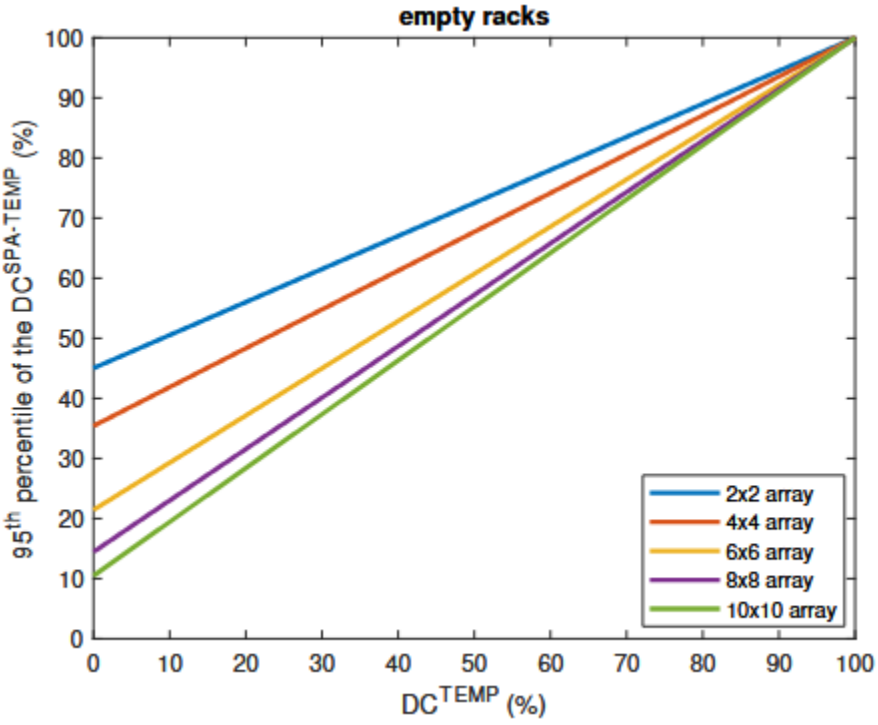

Figure 44: 95th percentile of the spatiotemporal duty cycle ($DC^{SPA-TEMP}$) (%) as a function of the temporal duty cycle (DC^{TEMP}) (%) for the five different arrays.

3.2.7.4 Conclusion

As a summary to this elaborate section, we can state that we evaluated 5G RF-EF mmWave exposure using five different MIMO array sizes (2x2, 4x4, 6x6, 8x8, and 10x10) in a realistic industrial scenario with two base stations at 28 GHz. We showed that the exposure of non-users compared to active users ranged from 1 (for 2x2 array) to 2.1 (for 10x10 array) orders of magnitude lower. We found that the maximum difference in exposure levels between user and non-user locations was achieved when a 10x10 array is used, with differences of around 10 dB. The spatiotemporal duty cycle was analyzed for an indoor industrial environment. The simulations showed that for the same connection time (i.e., Ts = 10s, 3% of the 6-minute time-averaged) the 95th percentile of the spatiotemporal duty cycle was reduced from 46.6% (2x2 array) to 11.6% (10x10 array), which represents a reduction of 6.4 dB of the exposure level. It was also demonstrated that the racks contents have little influence on exposure values and duty cycles (i.e., 2% lower spatiotemporal duty cycle for Ts = 10s and 10x10 array). In all studied cases, increasing the array size and reducing the connection time were effective strategies for lowering the spatiotemporal duty cycle. In the future, sub 6 GHz and future 6G FR3 frequencies can be investigated, also including human models.

3.2.8 Overall discussion and conclusion

This section has presented the simulation results for a large variety of scenarios. This brings together the various results and compares them. Figure 45 shows a cdf plot of the different FR1 scenarios presented above. It can be noticed that there is a relatively large spread between the simulated values. The lowest overall exposure is found in the Warehouse Germany scenario (see Section 3.2.1.1), with E_{50} and E_{95} values of 0.34 V/m and 1.06 V/m respectively. On the other hand, maximal values are found in the Port of Koper scenario (see Section 3.2.2), with E_{50} and E_{95} values of 8.29 V/m and 16.44 V/m respectively. Also, the office picocell scenario causes relatively large exposure values. The Lab WiFi scenario (for the static radiation pattern and for bystanders) lead to E-field levels that are comparable to Warehouse Germany and Production Hall scenarios, with a slight increase for actual users. The main reason for the high values in the Port of Koper and office picocell scenarios are the high antenna input powers (100 W and 20 W respectively), in combination with directional antennas.

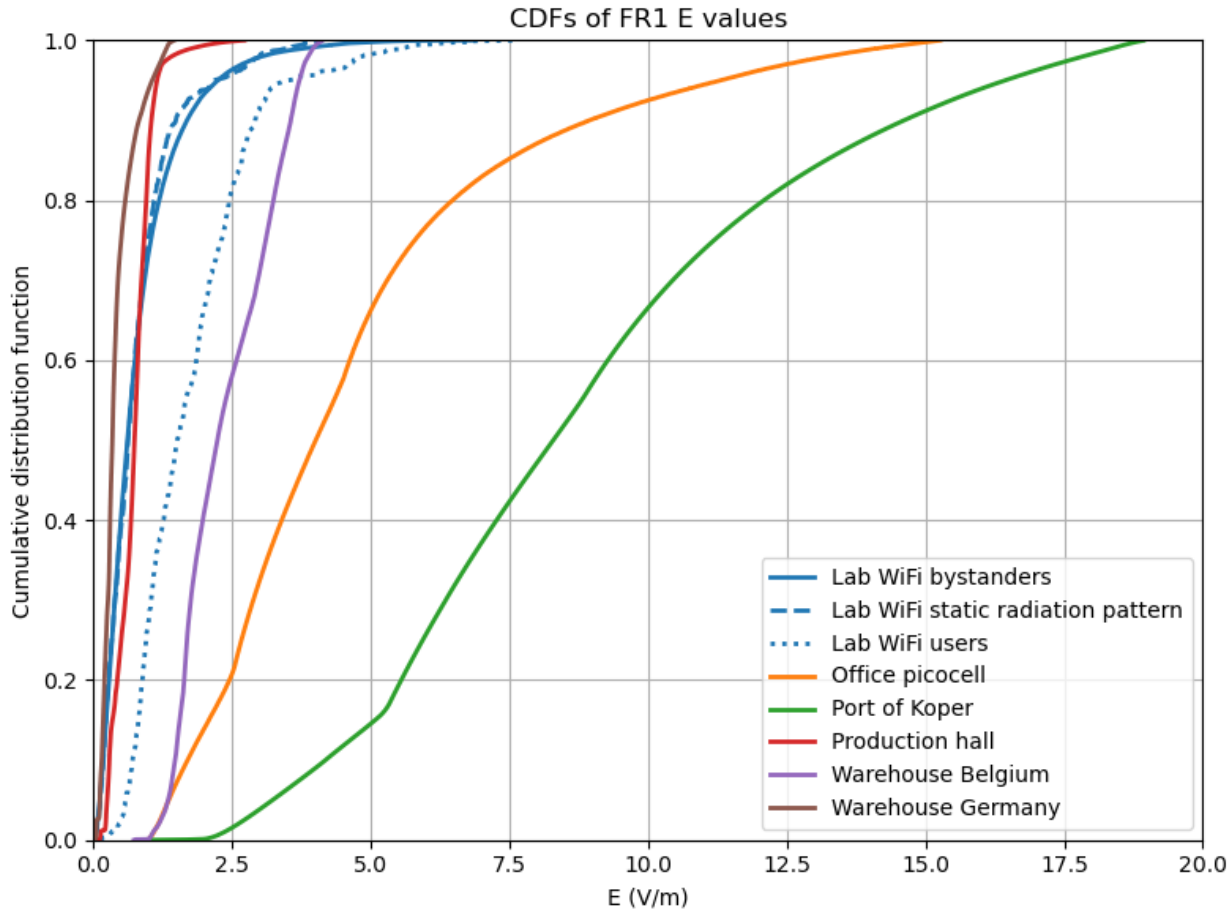

Figure 45. CDFs of E values in the different FR1 scenarios

Figure 46 shows a cdf plot of the FR2 scenarios presented above. The scenarios from Warehouse Belgium shows values converted to E for a clearer comparison with the FR2 lab scenario (see Section 3.2.6) and the FR1 scenarios. It shows that the FR2 lab scenario has higher maximal values and lower minimal values that the Warehouse Belgium scenario, despite having the same antenna input power of 30 dBm. The reason is that the FR2 lab scenario considers a fixed beam direction, while the Warehouse Belgium scenario averages out over the different user and non-user locations. The figure confirms that non-user exposure experiences limited influence from beamwidth, while narrower beams increase user exposure more significantly, as expected.

When comparing FR1 and FR2 exposure values, it is observed that simulated field levels are comparable.

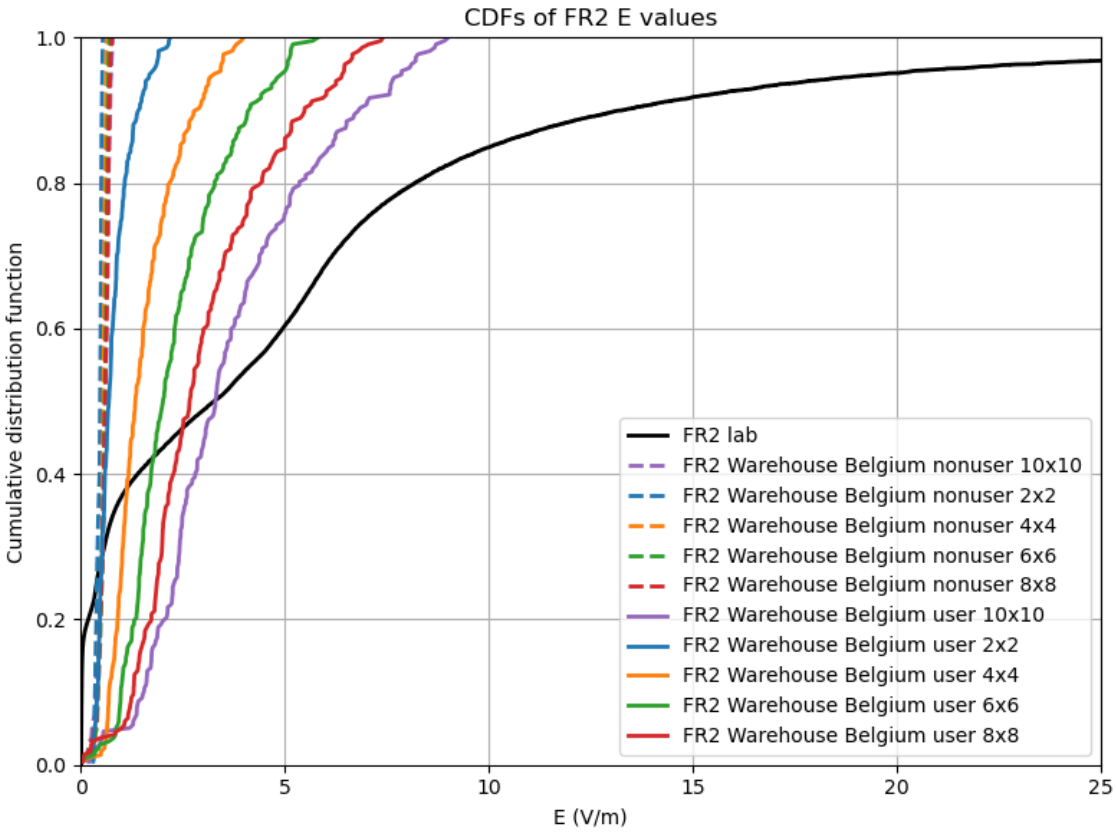

Figure 46. CDFs of E values in the different FR2 scenarios

FR 1		
Environment	**E_{50} (median E value)**	**E_{95} (maximal E value)**
Warehouse Germany	0.34	1.06
Production hall	0.74	1.14
Port of Koper	8.29	16.44
Office picocell	4.01	11.31
Warehouse Belgium	2.23	3.71
Lab WiFi users	1.51	3.52
Lab WiFi bystanders	0.61	2.24
Lab WiFi static radiation pattern	0.62	2.19
FR2		
Environment	**E_{50} (median E value)**	**E_{95} (maximal E value)**
Lab	3.27	19.69
Warehouse Belgium 2x2 users	0.69	1.69
Warehouse Belgium 4x4 users	1.34	3.28
Warehouse Belgium 6x6 users	2.02	4.93
Warehouse Belgium 8x8 users	2.67	6.41
Warehouse Belgium 10x10 users	3.29	7.86
Warehouse Belgium 2x2 non-users	0.47	0.52
Warehouse Belgium 4x4 non-users	0.55	0.62
Warehouse Belgium 6x6 non-users	0.59	0.67
Warehouse Belgium 8x8 non-users	0.59	0.71
Warehouse Belgium 10x10 non-users	0.59	0.74

4 Towards a generic model for exposure estimation

In this section, a generic model is developed to estimate RF exposure of employees in Smart Factories.

Specifically, in this task we investigated to what extent input parameters that are accessible and understandable to a layman/employer can be used to obtain a reliable estimate of the exposure (E field) in a certain (industrial) area. State-of-the-art numerical modelling and simulation tools were used in conjunction with machine learning approaches. Trained and tested with a large number of simulation scenarios and a selected set of experimental datasets, it forms a foundation for the exposure research community to add datasets, finetune the model or create new models. Such model could aid in informing industrial workers on exposure levels that are to be expected, without requiring complex software simulations or technical knowledge of the wireless setup.

4.1 Methodology

The approach consists of different steps.

First, we listed a set of candidate input parameters. These parameters were expected to exhibit a correlation with the overall exposure values in the considered area. These input parameters should be easily understandable (e.g., no use of datasheets, no technology-specific parameters, no path loss models or any technical knowledge required …). The output parameter (which we tried to estimate based on the inputs) is a metric that represents the (distribution of) exposure levels in the considered area.

In a next phase, we explored this input parameter space, retained those that show most correlation, varied their values and each time determined the corresponding output parameter values. This means that exposure output values were evaluated for a large variety of configurations, determined by their input parameters.

Next, all inputs and their output values were used to build a machine learning-based prediction model. Part of the dataset was used for model training, while another set was used for testing the model. Given the fact that constructing such models with multiple input parameters required a large dataset and that relatively little experimental 5G data is available, we built on exposure simulations in MatLab. However, we also linked the obtained generic model to some available experimental datasets.

Below, we elaborate on the different steps on the approach and their building blocks.

4.1.1 Input and output parameters

Here, we define candidate input parameters, as well as the output parameters we considered. Each prediction instance is represented by [**X Y**], with **X** the vector of input parameters and **Y** the

vector of output parameters. Initially, **X** is defined as a 11-dimensional vector (X1,X2,…,X11), and **Y** as a 3-dimensional vector (Y1,Y2,Y3). The **input parameters** were the following:

- X1= Size of object/area of the factory: the total evaluation area (in m², real value ϵ]0,+ ∞ [)
- X2= number of transmit sources or base stations (BS): the total number of transmitters in the evaluation area (unitless, integer value ϵ {1,2,3,..}). The more transmitters, the higher the expected exposure values.

- X3= density of sources: the number of square meters of area per deployed base station, i.e., X1/X2 (m², real value ϵ (0,+ ∞)). As X3 is redundant to X1 and X2, it was investigated if X3 only can be used and X1 and X2 omitted in the model, as we expect exposure values to mainly depend on base station *density,* rather than on the number of base stations.

- X4 = frequency: the frequency used by the base stations (GHz, real value ϵ {3.5, 2.4, 5.0, …}) (see 'additional notes' for link with 'technology'). Depending on frequency, the radio waves interact differently with their environment. Technology is not included as input, and our simulations do not account for 'technology'. However, as interface to the layman employer, we might use 'technology' (e.g., from dropdown menu) instead of 'frequency', with an internal translation to the model's 'frequency' parameter, although in case of technologies using multiple bands, further specification might be required.

- X5= base station height: height of the base station antennas above the ground level (m, real value ϵ (0, +∞)). For the sake of simplicity, it is assumed that all base stations are installed at the same height. Alternatively, we can use an average base station height if base stations are installed at different heights.

- X6= base station power: input power to the antennas of the base stations (dBW, real value ϵ (- ∞, +∞)). For the sake of simplicity, it is assumed that all base stations have the same power. Alternatively, we can use an average base station power.

- X7=antenna type: the antenna gain of the base stations' antennas (dBi, real value ϵ {2.15, 4.5, …}). Here, we restrict ourselves to two antenna types: an omnidirectional antenna when mounted on ceilings (gain = 2.15 dBi), and a half-omnidirectional antenna covering a 180° sector, as is mounted on walls (gain = 4.5 dBi). This is an approximation of the actual antenna gain, as laymen cannot be expected to input a full radiation pattern or have knowledge of antenna parameters. Therefore, we use the base station location (ceiling or wall) as a proxy for this value. Note that we also exclude beamforming from the analysis.

- X8=clutter area percentage: the percentage of floor area covered by clutter/objects (real value real value ϵ [0,1)). The employer could e.g., be asked to provide an approximation of the total area occupied by clutter (can be estimated more easily from his/her floorplan than

clutter area percentage), and then it can be internally converted to a clutter percentage suitable for the model input (by dividing by variable X1). Asking for clutter density as a textual input (e.g., light, medium, dense,…) is expected to be too subjective. The clutter height was set at 3.3 m (2/3 of the height of a typical 5 m ceiling).

- X9= dominant clutter material: the type of clutter that is dominant in the area: wood, metal, water, concrete; this value can be internally translated to the material's coefficient of reflection as input to the model (unitless, real value ϵ [0,1])

- X10= outer wall material: the material of the outer wall of the area: glass, metal, concrete, wood, brick, drywall; this value can internally translated to the material's coefficient of reflection as input to the model (unitless, real value ϵ [0,1])

- X11= ceiling height: the height of the ceiling (m, real value ϵ (3, + ∞))

As **output parameters**, we assumed the following three parameters:

- Y1=Median electric field value (median E over the entire area where no clutter is present).
- Y2=Maximal electric field value (E_{95} value (95^{th} percentile) over the entire area where no clutter is present).
- Y3=Kurtosis (tailedness of the distribution of electric field values over the entire area).

In an actual usage scenario, we could translate the median and/or E95 value to a textual/descriptive formulation for the employer (negligible, low, high, …). We opted for median and 95^{th} percentile E values as output instead of mean E values, as exceptionally high (simulated) E values close to the antennas would (wrongly) draw the mean E value to unrealistically high values.

4.1.2 Scenario simulations

To investigate the correlation between inputs and outputs and to eventually build the model, simulation configurations were executed, exploring the input parameter space. These simulations were executed in MatLab, based on environments created in Blender. This section describes how this dataset was built.

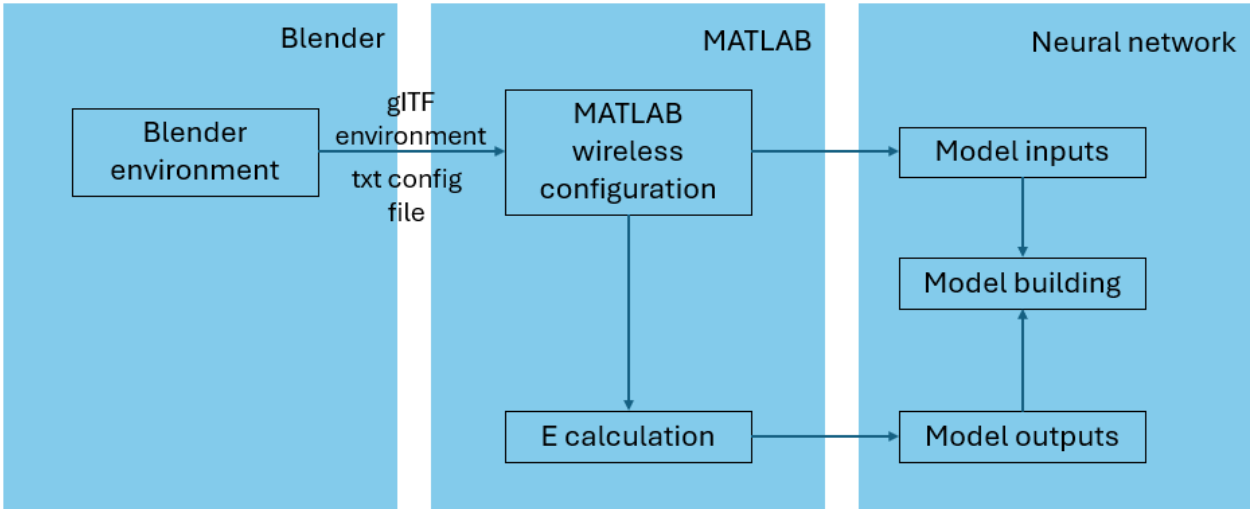

Figure 47. Flow graph for creating the generic model

4.1.2.1 Blender environment creation

Blender software – Blender is an open-source 3D modeling software widely used for creating detailed and customizable environments, making it particularly suitable for electromagnetic simulations. It allows users to assign different materials to objects, enabling accurate representation of electromagnetic properties such as reflection, which are critical for realistic simulation results. Blender supports exporting models in a variety of standard formats (e.g., OBJ, STL, FBX, glTF), allowing seamless integration with electromagnetic simulation tools. Additionally, its Python API enables the programmatic generation of complex scenes and large numbers of models.

Environment creation - For the creation of the environments, a Python script was developed that dynamically sets the dimensions of the indoor spaces. Each indoor space's length and width were randomly selected from a specified range, while its height was chosen from a set of predefined values (see Section 3.1.2.3 Simulation scenarios). The script also generates clutter objects that do not overlap and have a generic rectangular form. The script is both able to position the clutter objects in a random location in the area as to randomly position clutter objects in a typical aisle-like fashion, to resemble typical industrial environments with racks. Figure 48 shows two generated random environments: one with randomly positioned clutter objects (left) and one with more regularly positioned clutter objects (right). The number and dimensions of the clutter objects that were generated depend on the indoor space's dimensions and were randomly set in a way that fulfilled the requirement to create environments with clutter density ranging from 0% to over 50%. Following the creation of the clutter objects, the materials were assigned to the clutter objects and the outer walls.

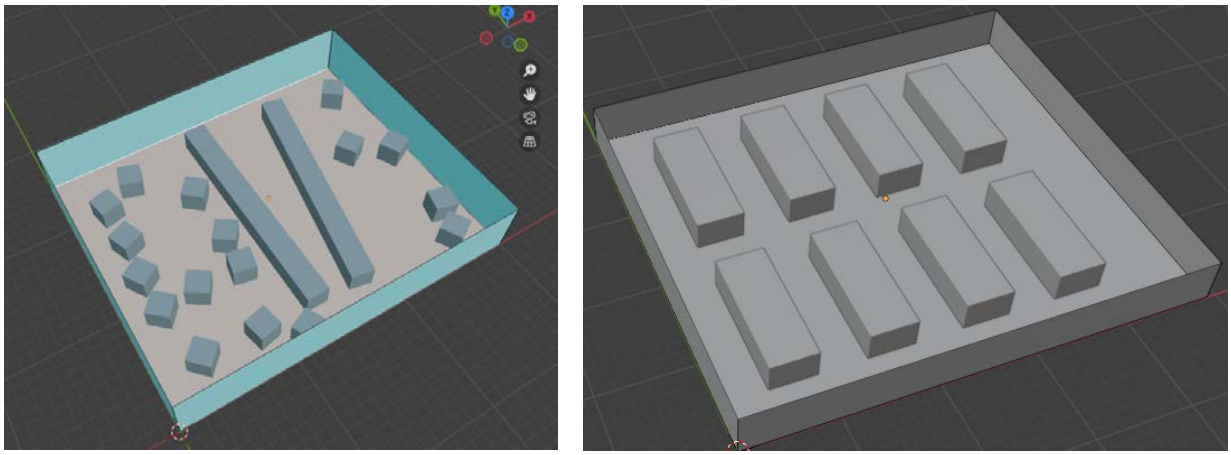

(a) (b)

Figure 48. Environments created with python script in Blender: a) randomly positioned clutter, b) regularly positioned clutter

Eventually, the Python script yielded a Blender environment, an area defined by its outer walls (X1, X10), a ceiling of a specified material (X10) and height (X11), and clutter objects (X8) made of a certain material (X9). This environment was exported in glTF format, which can be imported into MATLAB, where the electromagnetic simulations were performed. Additionally, the Blender script created a text file containing each 3D model's characteristics (e.g., dimensions, clutter positions), which was also imported into MATLAB and used to define several parameters of the electromagnetic simulations, such as the number and placement of BS and the position of the receiver grid points.

4.1.2.2 MATLAB electric-field calculation

For the electric field calculation, we used the MATLAB numerical tool using phasor sum described in Section 2.

In the cases where more than one BS is used, the total electric field is calculated as

$$E_{tot} = \sqrt{\sum_{i=1}^{N} E_i^2}$$

where E_i is the electric field caused by BS_i, and N is the total number of BS. In all simulations, we assume an evaluation height of 1.5m above ground level. For simplicity, we always assumed a DC of 100% so we don't account for duty cycle/traffic load/data usage as model input.

Several modifications were made to the numerical tool, as various parameters needed to be set and dynamically adjusted in order to vary all the input parameters of the generic model and obtain the full set of simulations. Here, the values for the number of base stations (X2) and their

frequency (X4), height (X5), transmit power (X6) and antenna type (X7) were determined, after which the BS are located on the map. X3 is automatically calculated from X1 and X2.

The position of the BS was dynamically set based on their number, the environment's dimensions, and the placement of clutter, in order to obtain realistic deployments. Finally, the grid positions where the electric field was calculated, were determined based on the environment area and the areas occupied by clutter. Figure 49 shows two of the generated environments, illustrating the clutter and base station placement.

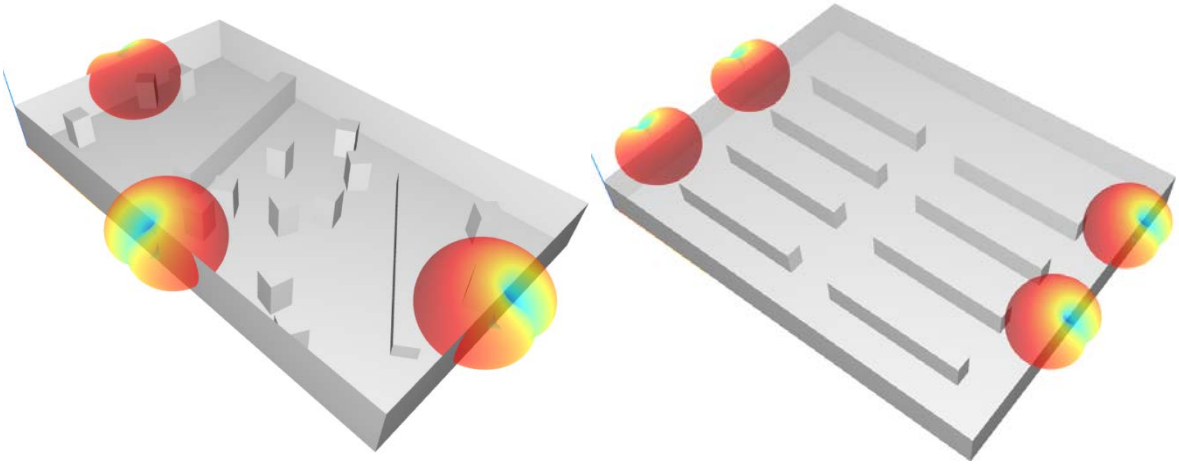

(a) (b)

Figure 49. a) Environment with randomly placed clutter and 3 base stations, b) Environment with regularly placed clutter and 4 base stations.

4.1.2.3 Simulation scenarios

To build and evaluate the generic model, a lot of [**X, Y**] data was required, meaning that many different configurations were required in which the 11 input parameters were varied. This section describes the scenarios that were simulated: the total amount of simulations and which input parameters were varied.

In a first phase, 12 800 different configurations were evaluated. 200 random factory layouts were created with a random length and width (X1) as described in Table 18, with a ceiling height of 5 m (X11) and with a random percentage of clutter (X8). These layouts were divided into 4 groups of 50, each assigned a unique combination of clutter (X9) and wall (X10) material. Within each group, we ensured that there were 10 configurations with 0–5% clutter, 10 with 5–10% clutter, and 10 with 20–25% clutter. These 200 unique models were then imported into MATLAB, where the BS were added, with their amount (X2) varying among four values, depending on the area of the environment. X3 was automatically calculated from X1 and X2. The BS frequency (X4) was set to either 3.5 or 26 GHz. The BS height (X5) varied across three values up to the factory ceiling

height of 5 m, depending on the antenna type. The Base Station power (X6) was varied among four values. The BS antenna type (X7) was selected from two options (wall or ceiling), which determined the corresponding radiation pattern (half-omnidirectional with a gain of 4.53 dBi and omnidirectional with a gain of 2.15 dBi respectively).

As in realistic deployments, the wireless installation will be configured to provide a realistic coverage percentage throughout the area. If more than 10% of the values received a signal level below -81 dBm (3.5 GHz) [Castellanos] (bandwidth of 120 MHz, with noise floor of -93 dBm, noise figure of 7 dB and SNR of 5 dB for MCS 7) or below -74.9 dBm (26 GHz) [Santana], the simulation was not withheld for further processing. In the first phase, this led to rejection of 2604 simulations or 20% of the total.

Based on the obtained results, we performed a second round of simulations, considering larger areas (X1) also including more clutter (X8), refining the BS power (X6) input parameter evaluations. 240 new environments are generated (X1, X8, X9, X10), with 2 amounts of base stations (X2) and 4 BS powers (X6). These were further varied with different BS heights (X5) up to the ceiling height (X11, 5 and 6 m) for wall and ceiling base stations (X7). This resulted in a set of 8640 simulations. In this second phase, 929 simulations or 11% were rejected.

Table 18. Input parameter ranges for the two sets of simulations

	1st set of simulations	**2nd set of simulations**
inputs	**range**	**range**
indoor space size: X1	440 - 2025 m^2 Random Length x Width (Length: 22-45m Width: 20 - Length)	462 - 2970 m^2 Random Length x Width (Length: 22-55m Width: 20 - Length)
BS number: X2	1, 2, 3, 4 1 and 2 (for 440 - 750 m^2 areas) 2 and 3 (for 750 - 1250 m^2 areas) 3 and 4 (for areas larger than 1250m^2)	1, 2, 3, 4 1 and 2 (for 440 - 750 m^2 areas) 2 and 3 (for 750 - 1250 m^2 areas) 3 and 4 (for areas larger than 1250m^2)
BS density: X3	220 - 750 m^2 / BS derived from X1 and X2	231 - 990 m^2 / BS derived from X1 and X2
Frequency: X4	3.5, 26 GHz	3.5 GHz
BS height: X5	3, 4, 5 m (varied only for wall antennas / for ceiling antennas, BS height is the ceiling height)	3, 4, 5, 6 m (varied only for wall antennas / for ceiling antennas BS height is the ceiling height)

BS power: X6	-20, -10, 0, 10 dBW (i.e., 0.01, 0.1, 1, 10 W)	-7, -3, 0, 3 dBW (i.e., 0.2, 0.5, 1, 2W)
antenna type (directivity): X7	2.1, 4.53 dBi	2.1, 4.53 dBi
clutter density: X8	0 - 25 %	2.2 - 62.5 %
clutter material (reflectivity): X9	0, 0.146, 1 (0 for no-clutter, 0.146 for wooden clutter, 1 for metal clutter)	1 (only metal clutter)
wall material (reflectivity): X10	0.046, 0.348 (0.046 for glass, 0.348 for concrete)	0.348 (only concrete walls)
ceiling height: X11	5	5, 6

4.1.2.4 Configuration settings: accuracy vs. calculation time

For building a solid machine learning model, we needed a lot of training data and hence, a lot of simulations, as explained in the previous section. Therefore, a good tradeoff must be found between the calculation time per simulation and the achieved simulation accuracy. As more **reflections** and/or **diffractions** are allowed in the simulation, accuracy is expected to go up, but calculation time as well. Therefore, for a set of four largely different simulation scenarios, the output parameters E_{50} and E_{95} were calculated, as well as the calculation time. This allowed us to determine simulation settings that strike a good balance between accuracy and calculation time.

Similarly to the number of interactions allowed the number of receiver points in the area at which the E value is calculated had an impact on calculation time. Therefore, we investigated the difference in $E_{50/95}$ values for a **receiver grid** with spatial **resolutions** of 10, 20, 50, 100, and 200 cm. Although a sparse grid reduces calculation time, it might not be able to catch all local differences in E values, having an impact on the representativeness of the E_{50} and (particularly) E_{95} outputs. Therefore, we determined the $E_{50/95}$ values as a function of the grid size resolution for the four scenarios. For a 'worst-case' environment (lot of clutter), we calculated the output (median E), and determined to what extent coarser grids still gave the same output.

4.1.3 Machine learning approach

As generic model, we used a fully connected neural network, where each neuron in one layer is connected to every neuron in the next. These networks consist of an input layer, one or more hidden layers, and an output layer. Each neuron applies a weighted sum followed by a non-linear activation function to capture complex patterns in the data. The hyper-parameters used are shown in the table below.

Hyper-parameter	Value
Number of neurons in each layer	20, 20, 20, 3
Activation function	Relu
Optimizer	Adam
Initial learning rate	0.005
Loss function	mean_squared_error
Train and test ratio	8:2

4.2 Results

This section first describes the results of the determination of the configuration settings, based on a trade-off between calculation accuracy and calculation time. The presented settings were then adopted in the construction and evaluation of the generic model, of which the results are presented in Section 3.2.2.

4.2.1 Configuration settings

Figure 50 shows E50, E95, and the calculation time as a function of the number of interactions (reflections/diffractions) allowed. As the number of interactions increases, calculation time increases exponentially. The obtained E values remained relatively stable though. Therefore, as a suitable tradeoff, we allowed 2 reflections for the remainder of the analysis.

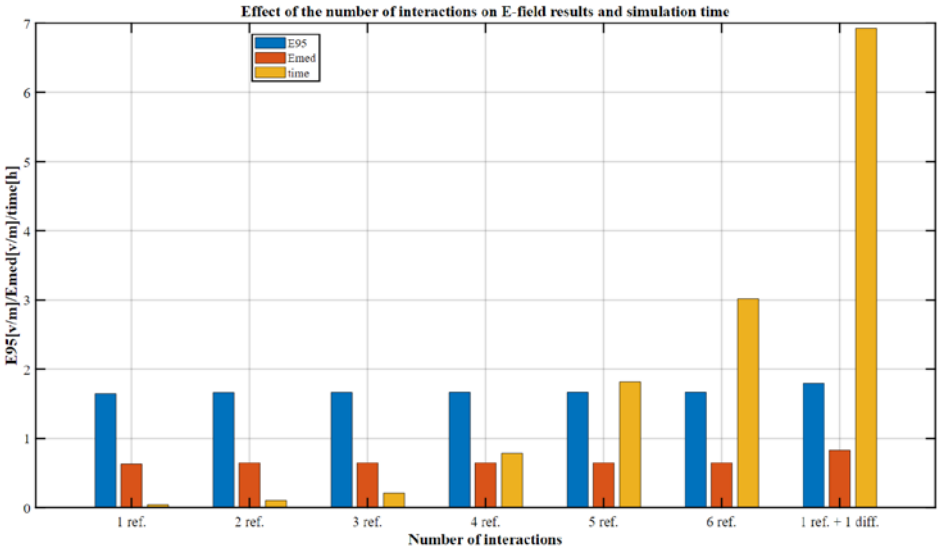

Figure 50. Comparison of E50, E95, and calculation time for different amounts of interactions allowed.

Figure 51 shows E_{50} and E_{95} as a function of the **grid size** resolution (in m) for four simulation scenarios. For the worst-case scenario (scenario 1), the differences remained below roughly 4% when choosing a grid size of 1 m, compared to smaller grid sizes. Therefore, we opted for a 1 m grid size as a good tradeoff between accuracy and calculation time.

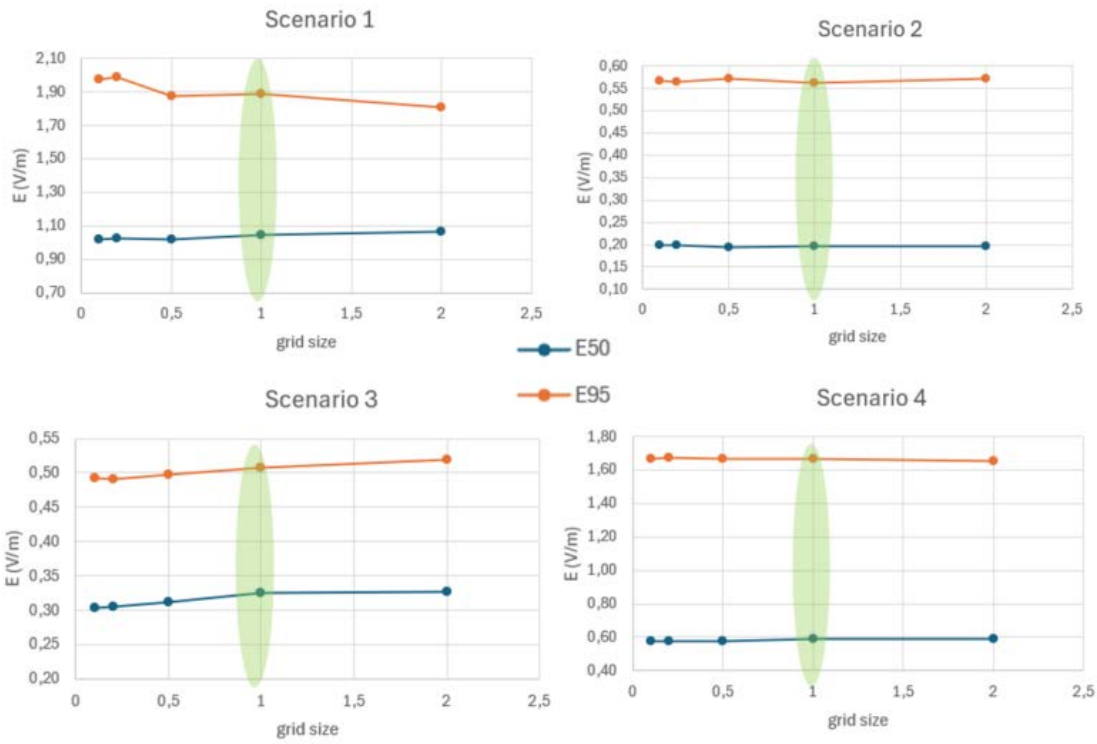

Figure 51. Comparison of E50 and E95 for different receiver grid sizes.

4.2.2 Generic model results

This section– based on the dataset generated as described in Section 3.1.2.3- first describes the results of the correlation analysis, followed by a discussion on the performance of the generic model.

4.2.2.1 Correlation analysis

The Pearson correlation coefficient measures the strength and direction of the linear relationship between two variables. The correlation analysis between all inputs variables and all potential output variables are shown in Table 19 below. We observed strong correlations between transmit power (X6) and E_{50} and E_{95} in the outputs. Some significant correlations were also observed from density of transmitters (X3), transmitter height (X5), type of antenna (X7), and density of clutter (X8). The correlation analysis confirmed that X3 (density of transmitters) provides the same information as the evaluation area (X1) and the number of transmitters (X2). The correlation between inputs and outputs revealed the essential parameters that could be used in machine learning model building. As a conclusion to this analysis, we retained the parameters in red as the essential input features for building the model: X3, X5, X6, X7, X8.

Table 19. Correlation table between all inputs and outputs.

	Area	Num_ Trans	Den_ Trans	Fre_ Trans	H_ Tran	P Tran	Type_ Ant	Den_ Clutter	Mat_ Clutter	Mat_ Wall	H_ Ceiling	E_{50}	E_{95}	kurtosis
Area	1.000	0.709	0.596	-0.228	0.065	0.074	0.029	0.344	0.250	0.236	0.296	-0.086	-0.080	0.033
Num_Trans	0.709	1.000	-0.104	-0.134	0.039	0.044	0.017	0.247	0.153	0.127	0.173	0.084	0.001	-0.135
Den_Trans	0.596	-0.104	1.000	-0.152	0.043	0.050	0.019	0.181	0.174	0.175	0.199	-0.224	-0.116	0.236
Fre_Trans	-0.228	-0.134	-0.152	1.000	-0.082	-0.089	-0.026	-0.226	-0.281	-0.273	-0.357	0.068	0.065	0.040
H_Tran	0.065	0.039	0.043	-0.082	1.000	0.027	-0.443	0.060	0.084	0.082	0.242	-0.021	-0.212	-0.543
P_Tran	0.074	0.044	0.050	-0.089	0.027	1.000	0.009	0.074	0.092	0.089	0.116	0.721	0.827	-0.018
Type_Ant	0.029	0.017	0.019	-0.026	-0.443	0.009	1.000	0.048	0.027	0.026	0.055	-0.023	0.091	0.316
Den_Clutter	0.344	0.247	0.181	-0.226	0.060	0.074	0.048	1.000	0.270	0.227	0.346	-0.248	-0.054	0.100
Mat_Clutter	0.250	0.153	0.174	-0.281	0.084	0.092	0.027	0.270	1.000	0.280	0.367	-0.099	-0.074	-0.012
Mat_Wall	0.236	0.127	0.175	-0.273	0.082	0.089	0.026	0.227	0.280	1.000	0.357	-0.073	-0.073	-0.035
H_Ceiling	0.296	0.173	0.199	-0.357	0.242	0.116	0.055	0.346	0.367	0.357	1.000	-0.088	-0.105	-0.079
E_Median	-0.086	0.084	-0.224	0.068	-0.021	0.721	-0.023	-0.248	-0.099	-0.073	-0.088	1.000	0.835	-0.144
E_95per	-0.080	0.001	-0.116	0.065	-0.212	0.827	0.091	-0.054	-0.074	-0.073	-0.105	0.835	1.000	0.059
kurtosis	0.033	-0.135	0.236	0.040	-0.543	-0.018	0.316	0.100	-0.012	-0.035	-0.079	-0.144	0.059	1.000

4.2.2.2 Model performance

Based on the correlation analysis and the approach described in Section 3.1.3, a generic ML model was built, with input parameters X3, X5, X6, X7, X8 and output parameters Y1, Y2, Y2. For the fully connected neural network model, the training and testing performance are shown in the scatter plots shown in Figure 52. A good prediction can be observed from E50 (Figure 52 top left) and E95 (Figure 52 top right) while the kurtosis shows larger dispersion (Figure 52, bottom), suggesting weaker reliability for this higher-order statistic.

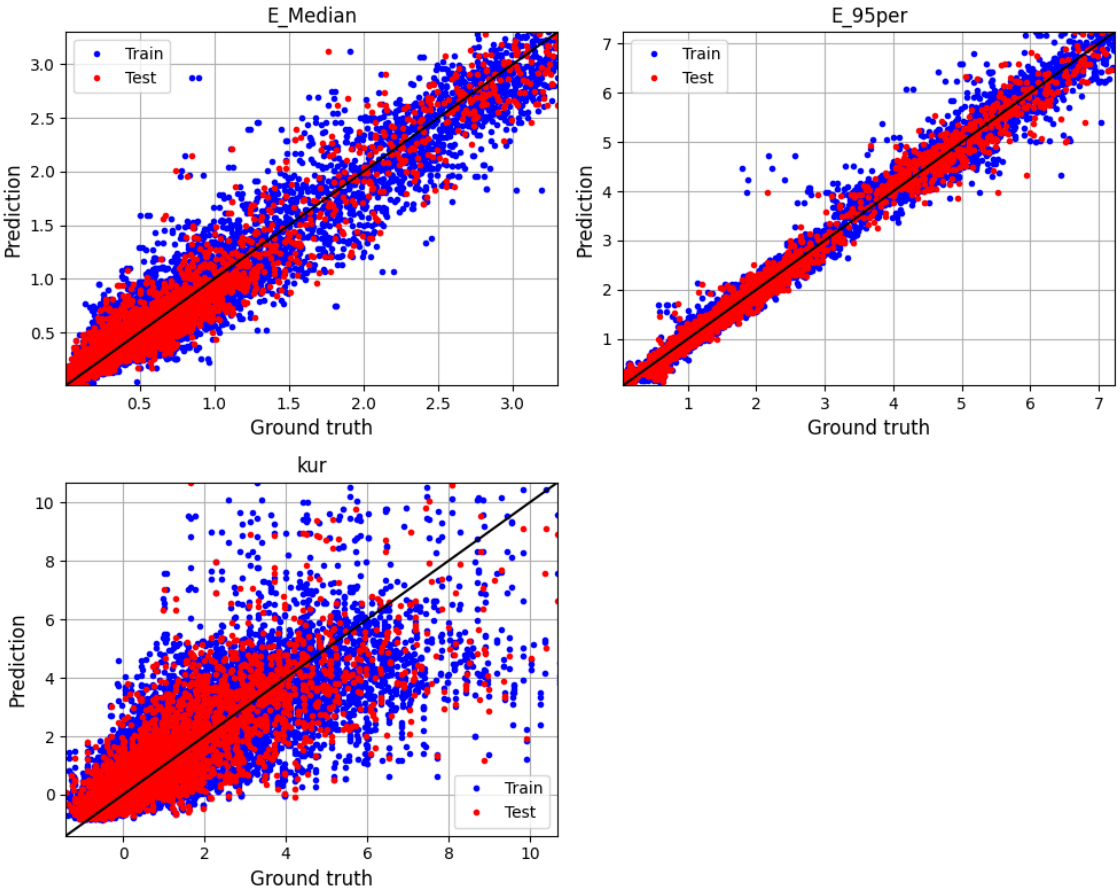

Figure 52. Scatter plots of predicted values vs. ground truth values for the three output variables.

In terms of training and testing performance metrics, we have a mean squared error (MSE) and R^2 for training and testing shown in the table below. MSE measures the average squared difference between predicted values and actual target values. R^2 measures how well the model explains the variance in the target variable. It ranges from 0 to 1, where 1 means the model perfectly explains the variance, 0 means it performs no better than predicting the mean, and negative values indicate worse performance than the mean predictor.

The model demonstrates strong predictive performance for both **E_Median** and **E_95per**, with low MSE and high R^2. For E_Median, the R^2 is around 0.95 for both training and testing, indicating the model explains 95% of the variance with consistent generalization. These results confirm that the model captures the underlying trends very accurately, especially for percentile-based measures.

	E_{50}	E_{95}
MSE-Training	0.02672	0.03028
MSE-Testing	0.02619	0.02704
R^2-Training	0.94969	0.98969
R^2-Testing	0.94948	0.99048

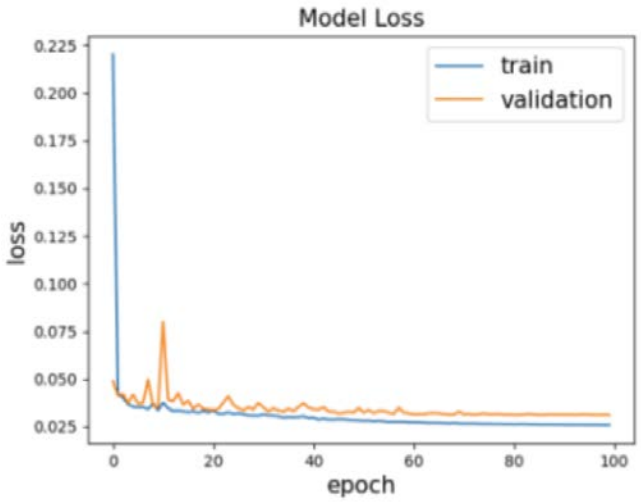

Figure 53. training and validation loss as a function of number of epochs

The loss graph of Figure 53 shows the training and validation loss across 100 epochs. This indicates that the model is learning effectively, with no strong signs of overfitting since the training and validation losses remain close throughout training.

5 Publications

P. Gajšek, C. Apostolidis, D. Plets, T. Samaras, B. Valič, "EMF Exposure of workers due to 5G private networks in Smart Industries", *mdpi Electronics, Special Issue on Innovations in Electromagnetic Field Measurements and Applications*, Impact Factor 2.6, accepted.

Y. H. Santana, G. G. Nieto, T. Van de Steene, R. Martinez Alonso, L. Martens, W. Joseph, D. Plets, "User and Non-User 5G mmWave EMF Exposure Analysis in an Industrial Environment", *IEEE Transactions on Green Communications and Networking*, Impact Factor 6.7, major revisions.

6 References

[5G-LOGINNOV] 5G-LOGINNOV project website, https://5g-loginnov.eu/

[Castellanos] G. Castellanos, S. De Gheselle, L. Martens, N. Kuster, W. Joseph, M. Deruyck, S. Kuehn, "Multi-objective optimisation of human exposure for various 5G network topologies in Switzerland", *Computer Networks*, Volume 216, 2022, 109255, https://doi.org/10.1016/j.comnet.2022.109255.

[ICNIRP] International Commission on Non-Ionizing Radiation Protection, 2020. Guidelines for limiting exposure to electromagnetic fields. Health Physics 118, 483524. URL: http://dx.doi.org/10.1097/HP.0000000000001210, doi:10.1097/hp.0000000000001210.

[ITU] Series, P., 2015. Eects of building materials and structures on radiowave propagation above about 100 mhz. recommendation itu-r , 2040-1

[Plets] Plets, D., Joseph, W., Vanhecke, K. *et al.* Coverage prediction and optimization algorithms for indoor environments. *J Wireless Com Network* 2012, 123 (2012). https://doi.org/10.1186/1687-1499-2012-123

[Santana] Santana, Y.H., Martinez Alonso, R., Guillen Nieto, G., Martens, L., Joseph, W., Plets, D., 2024. 5g mmwave network planning using machine learning for path loss estimation. IEEE Open Journal of the Communications Society 5, 3451-3467. URL: http://dx.doi.org/10.1109/OJCOMS.2024.3405742, doi:10.1109/ojcoms.2024.3405742.

[Shikantsov] Shikhantsov, S. and Thielens, A. and Vermeeren, G. and Martens, L. and Demeester, P. and Joseph, W., "User and non-user RF-EMF exposure to the downlink Zero-Forcing transmission of distribute Massive MIMO in an industrial environment", *BioEM 2022, the 1st Annual Meeting of BioEM Society, Proceedings*, pp. 405-410. URL: https://www.bioem2022.org/.

[Shikantsov2023] Shikhantsov, S. and Thielens, A. and Aerts, S. and Verloock, L. and Torfs, G. and Martens, L. and Demeester, P. and Joseph, W., 2020. Ray-tracing-based numerical assessment of the spatiotemporal duty cycle of 5g massive mimo in an outdoor urban environment. Applied Sciences 10, 7631. URL: http: //dx.doi.org/10.3390/app10217631, doi:10.3390/app10217631.3273475, doi:10.1109/temc.2023.3273475.